SACLANTCEN REPORT
serial no: SR-315

SACLANT UNDERSEA RESEARCH CENTRE REPORT

BURIED MINE DETECTION AND CLASSIFICATION (RESEARCH SUMMARY 1996-1999)

A. Maguer, W.L.J. Fox, A. Tesei, E. Bovio, S.Fioravanti

July 1999

The SACLANT Undersea Research Centre provides the Supreme Allied Commander Atlantic (SACLANT) with scientific and technical assistance under the terms of its NATO charter, which entered into force on 1 February 1963. Without prejudice to this main task – and under the policy direction of SACLANT – the Centre also renders scientific and technical assistance to the individual NATO nations.

SACLANT Undersea Research Centre
Viale San Bartolomeo 400
19138 San Bartolomeo (SP), Italy

tel: +39-0187-5271
fax: +39-0187-527.420

e-mail: library@saclantc.nato.int

NORTH ATLANTIC TREATY ORGANIZATION

Buried mine detection and classification (Research Summary 1996-1999)

A.Maguer, W.L.J.Fox, B.Zerr,
A.Tesei, E.Bovio and S.Fioravanti

The content of this document pertains to work performed under Project 03-A of the SACLANTCEN Programme of Work. The document has been approved for release by The Director, SACLANTCEN.

Jan L. Spoelstra
Director

SACLANTCEN SR-315

intentionally blank page

Buried mine detection and classification
(Research Summary 1996-1999)

A.Maguer, W.L.J.Fox, B.Zerr, A.Tesei,
E.Bovio and S.Fioravanti

Executive Summary: Mines which are completely buried in sandy ocean sediments are considered to be undetectable and unclassifiable by conventional high frequency (of the order of hundreds kHz) minehunting sonars due to the very low levels of energy transmitted into the sediment at the low grazing angles used for minehunting. For classification, high-frequency approaches based on analysis of target acoustic shadow can not be exploited for buried targets. The use of lower frequency sonars [2-16 kHz], at grazing angles above and below the critical angle of "total reflection" off the water-sediment interface, is investigated, in order to enhance buried mine detection and classification performance. This report describes research at SACLANTCEN since 1996.

The detection of buried targets is effective at above critical angle, but provides very low area coverage which is limiting from an operational point of view. At subcritical angles, detection becomes difficult. Significant gains (of the order of 8 dB) in signal-to-reverberation ratio below critical angle were obtained either by emphasizing a relatively narrow band of frequencies at the lower end of the transmitted bandwidth (below 3 kHz) or by using larger physical array or synthetic array processing which improves the sonar resolution. Simulations, using the results obtained on sound penetration into sediment, have shown that very low frequencies (of the order of 0.5-1 kHz) are essential to the detection of buried targets at very low grazing angles and that detection at those frequencies will only be effective for shallow buried targets.

A new method for low-frequency target classification, based on multiple-aspect target echo analysis in time and frequency domains, is proposed. This method considers both the rigid and resonance responses to discrimate between man-made objects and natural objects, such as rocks. The classification result is provided on the basis of estimation of external shape and internal target properties. This low-frequency approach could allow therefore discrimination between objects of the same shape and size but with different internal structures. Its potential was demonstrated on simulated and real data (exercise mine, cylinders, spheres and rocks) for proud targets and buried spheres.

Future modelling and experiments will be dedicate to the design (in terms of central frequency, directivity and bandwidth) of a sonar to detect and classify buried mines (of more complex shapes) at operationally acceptable ranges.

intentionally blank page

Buried mine detection and classification
(Research Summary 1996-1999)

A.Maguer, W.L.J.Fox, B.Zerr, A.Tesei,
E.Bovio and S.Fioravanti

Abstract: The applicability of low-frequency sonar (2-16 kHz) to buried mine detection has been investigated. Experiments were performed on sound penetration into sediment, buried target detection and broadband multiple aspect classification. The results of the experiments are given in this report and compared with modelled results.

One of the main results is our success in understanding the physical mechanisms contributing to subcritical penetration into sediment. It has been demonstrated that the evanescent wave was dominant in the lower frequencies [2-5 kHz] of our bandwidth of interest [2-16 kHz]. Roughness scattering dominates at higher frequencies (above 5 kHz) for our bottom type (RMS roughness 1.5 cm, cross-ripple correlation length 25 cm). Although roughness scattering has been shown to be one mechanism for explaining *"anomalous"* penetration into sediment, its potential for detection and classification of buried objects is unclear due to the low level and the lack of coherence of the received signals. It is demonstrated that sound speed variation with frequency, and therefore variation of the critical angle versus frequency, could exist for permeable sandy bottoms, which could influence the design of a buried mine sonar.

The detection of buried targets is shown to be very effective at above the critical angle. At subcritical angles, detection becomes difficult. Significant gains in signal-to-reverberation ratio below critical angle were obtained either by emphasizing a relatively narrow band of frequencies at the lower end of the transmitted bandwidth (below 3 kHz) or by using a larger physical array or synthetic array processing which improve the sonar resolution. Simulations have shown that lower frequencies (of the order of 0.5-1 kHz) are essential to the detection of buried targets at low grazing angles and that the detection at those frequencies will only be effective for shallow buried targets.

A method based on multiple-aspect target echo analysis in time and frequency domains, which considers the rigid and resonance responses is presented. Its potential was demonstrated in simulation and on real data (exercise mine, cylinders and rocks) for proud targets and for buried spheres.

Keywords: seafloor scattering ∘ sound penetration ∘ Kirchhoff theory ∘ small perturbation theory ∘ evanescent wave ∘ detection ∘ synthetic aperture processing ∘ target classification ∘ tomography ∘ resonance scattering analysis ∘ target scattering modelling ∘ minehunting ∘

Contents

1

Introduction

The detection and classification of buried mines in ocean sediments is perceived as an operational shortfall. High-frequency (of the order of hundreds kHz) conventional minehunting sonars are of limited usefulness in these conditions, due to very low levels of energy transmitted into the sediment at the low grazing angles used for mine detection and the absence of shadow images for mine classification.

Detection is a particular problem in the case of hard bottoms (sand) characterized by a sound speed greater than sound speed in water and a critical angle below which, according to the classical reflection theory, "total reflection" will occur off the sediment interface and therefore very low levels of sound will penetrate into the sediment. While the detection in softer bottoms (mud, silt) is feasible, the classical high-frequency classification approach based on target echo analysis and shadow imaging will fail.

As the attenuative effect of sediment is reduced at lower frequencies, previous work on buried object detection sonar (around 20-30 kHz) has concentrated on high grazing angle insonification (above the critical angle of "total reflection" off the sediment interface). Detection performance was good even for deeply buried targets notwithstanding the high false alarm rate and a small area coverage.

In order to increase area coverage, the use of even **lower frequency sonars (center frequency (10 kHz) and higher fractional bandwidth (2-20 kHz))** was investigated, at grazing angles **above and below** the critical angle. This approach should allow better penetration both into the sediment and into elastic targets [1]. Consequently, target backscattering characteristics could be exploited for either proud or, partly or completely buried objects. In order to gather more pertinent information from the object echo and therefore to achieve better classification, it was decided to exploit **aspect dependence in time and/or frequency** of target backscattering in the frequency band (2-20 kHz). The aspect variation of target backscattering could be for example acquired by an Autonomous Underwater Vehicle (AUV) circum-navigating the target. In this frequency band, sound waves penetrate the target and the backscattered waves carry information relative to the external shape and internal properties (material and structure) of the object. Analysis of their

[1] For the mines considered here, this frequency range [2-20 kHz] corresponds to ka range where elastic contributions are significant and comparable to rigid contributions.

variation with aspect and frequency will allow classification into natural objects and man-made objects and identification from estimation of their geometrical and elastic characteristics. A key point of the target classification approach selected was the extensive work that was performed, in parallel to and interacting with the development of the classification techniques, on the object/waveguide scattering modelling [1] which extensively contributes to the development of the proposed **model-based** classification approach.

In the case of a buried mine sonar, in addition to the classical parameters necessary for the design of a proud mine system, two-way absorption loss into the sediment is an additional parameter which has to be known, in order to achieve a correct design of a detection system. Although in the case of supercritical insonification, the theory of sound propagation into sediment is well known and allows a complete system design, this is not the case for subcritical penetration into the sediment, where the theory is not yet completely understood. Different theories have been formulated (bottom roughness, Biot slow wave, narrow beamwidth, volume inhomogneities) in addition to the basic evanescent theory to explain the subcritical penetration into the bottom, with, however, no precise quantification of each phenomenon in relation to the others.

Section 2 is dedicated to the description of the results obtained on subcritical penetration into the sediment. Experimental results and their comparison to modelled results are given. It is shown that two main mechanisms (evanescent coupling and roughness scattering) are responsible for subcritical penetration into the sediment. It is demonstrated that variation of the critical angle *versus* frequency may exist for permeable sandy bottoms, a fact which could influence the design of a buried mine sonar.

Section 3 describes the results obtained for the detection of buried targets as a function of frequency, grazing angle and burial depth. Experimental results are shown which demonstrate the efficiency of detecting buried mines in the frequency band 2-16 kHz above critical angle. At subcritical angles, detection becomes difficult but can be improved either, by emphasizing a relatively narrow band of frequencies at the lower end of the transmitted bandwidth (below 3 kHz), or by using a larger physical array or synthetic array processing which improves the sonar resolution. Preliminary simulation shows that low frequencies (of the order of 500 Hz-1 kHz) are mandatory for the detection of buried targets at very low grazing angles and that detection at those frequencies will only be effective for very shallow buried targets.

Section 4 describes the methodology proposed for the low-frequency classification of mines, either proud or buried. The proposed approach is based on multiple-aspect target echo analysis in the time and frequency domains and combines the analysis of the specular reflection and potential diffraction effects (rigid response), and the so-called resonance response, in the case of man-made elastic objects having

particular symmetries (e.g., bodies of revolution). Experimental results are given which demonstrate the potentiality of the proposed method for both free-field and proud targets. Preliminary results with buried spheres are also given.

Section 5 summarizes the effort and gives directions for future work.

2

Subcritical sound penetration into sediments

In a reverberation-limited environment the expression for the signal-to-reverberation ratio, SR, is expressed as:

$$SR = TS - AL - BS - 10\log A. \tag{1}$$

where TS is the target strength, AL is the two-way absporption loss into the sediment, BS is the bottom backscattering and A is the insonified bottom area.

This equation shows the importance of perfect knowledge of two-way absorption loss AL into the sediment (including the loss at the water-sediment interface) for the design of a buried mine system.

2.1 Theory

According to reflection theory for a flat interface, the refracted wave into the sediment below the critical angle of "total reflection" off the sediment interface, becomes an inhomogeneous wave, **evanescent**, decreasing exponentially (i.e. linearly in dB) with frequency, burial depth and grazing angle [2].

From the reflection theory of plane waves in discretely layered media, according to the geometry shown in Fig. 1, the refracted wave in the lower medium (that means within the sandy bottom) can be written, for an incident plane wave of time dependence $\exp(-j2\pi ft)$ and unit pressure amplitude, as :

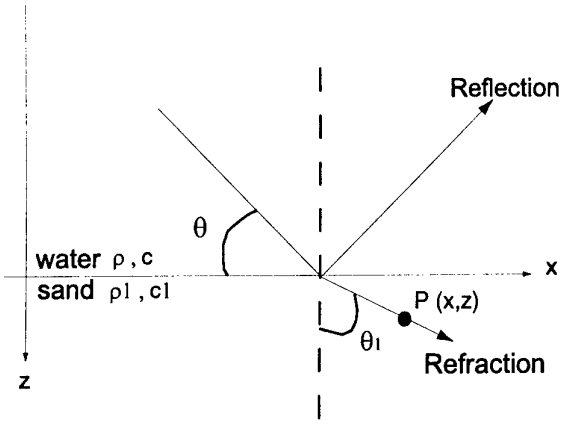

Figure 1 *Refraction and Reflection of a plane wave at the boundary between two fluid media (water and sand). Upper medium: sound speed c, density ρ; lower medium: sound speed c_1, density ρ_1.*

$$P(f,z) = \frac{2m\sin\theta}{m\sin\theta + \sqrt{n^2 - \cos^2\theta}} \exp\left[jkx\cos\theta + jk\sqrt{n^2 - \cos^2\theta}z\right]. \qquad (2)$$

Here, with the water being the reference, $m = \rho_1/\rho$ is the sediment density ratio, $n = c/c_1$ is the normalized index of refraction of the sediment, and θ is the incident grazing angle. k is the wave number equal to $2\pi f/c$. Attenuation in the bottom is taken into account by letting the index of refraction being complex, $n = n_r(1 + j\delta)$, where δ is the *loss tangent*, which relates to the the *attenuation coefficient* α in dB/λ, as $\alpha = 54.58\delta$ [3].

For sound travelling from the ocean to a sediment bottom, when c_1 is greater than c (which is the case for a sandy bottom), there is the possibility of "total reflection". Total reflection occurs at grazing angles θ_1 lower than θ_c, where θ_c is the critical angle defined by:

$$\theta_c = \arccos(c/c_1). \qquad (3)$$

At subcritical incidence, $\cos\theta > n$, the bottom field becomes evanescent and decreases exponentially (i.e. linearly in dB) with frequency, burial depth z and grazing angle:

$$P(f,z) = \frac{2m\sin\theta}{m\sin\theta + j\sqrt{\cos^2\theta - n^2}} \exp\left[jkx\cos\theta - k\sqrt{\cos^2\theta - n^2}z\right]. \qquad (4)$$

For sandy sediments the critical angle can be in the $20° - 30°$ range, which suggests that penetration at lower grazing angles may be limited.

Considering a sonar at a height H from the bottom, the range obtained for a grazing angle θ is given by:

$$r = H/\tan(\theta) \tag{5}$$

The range obtained, for a sandy bottom, within the critical angle, will therefore give a bottom area coverage of the order of 2.5 times the height of the sonar, which is limiting from an operational point of view.

Several researchers [4], [5] have reported "anomalously" high levels of sound penetration into ocean sediments at low grazing angles (which could consequently enhance detection range) when compared to basic theory. Competing hypotheses have arisen in order to explain this effect. Several theoretical explanations were hypothesized for this phenomenon, including:

1. the **roughness** of the water-sediment interface, which diffracts energy into the sediment [6],
2. the effect of using a **narrow beamwidth** [7],
3. the porous nature of sediment which leads to a second "slow" compressional wave (**Biot wave**) [8],
4. the **volume inhomogeneities** within the sediment that scatters the evanescent wave (propagating along the water/sediment interface) into the sediment [9]-[12].

The roughness of the water-sediment interface was identified as a candidate phenomenon contributing to subcritical penetration into the sediment. Seabed bottoms are often featured with rough interfaces due to the interaction of currents with the water-sediment interface. This interaction may be very strong, commonly producing relatively large, oriented, quasi-periodic features, i.e ripple fields. The common assumption is to consider that the incident wave will also be scattered into the sediment due to the fact that local facets of the insonified area possess grazing angles above critical, contributing to sediment penetration.

Subcritical penetration of narrow Gaussian beams into a sandy bottom was demonstrated in [7]. The explanation given was a simple consequence of the angular spectra

associated with narrow beams. A narrow beam is not a plane wave but more a composite of many plane-wave components subject to different reflectivity conditions at the interface.

The Biot theory assumes a fluid-saturated porous model which predicts the existence of two compressional waves and one shear wave. One of the two compressional waves has a lower sound speed than the water sound speed, which means the absence of a critical angle for this type of *slow* wave and penetration into sediment even at low grazing angle conditions.

Subcritical angle penetration was examined by conducting experimental and modelling studies in order to identify the mechanism(s) by which anomalously high levels of energy are transmitted into the sediment.

2.2 Experimental results

In the first experiment, (June 97) acoustic energy generated in the frequency band 2-16 kHz, using a parametric source TOPAS (primary frequency 40 kHz), was directed toward a sandy seabottom, where two hydrophones were buried at 30 cm and 60 cm in the sediment.

For the second experiment (December 97), an array of 14 buried hydrophones (at burial depths 5 cm, 25 cm and 45 cm) was used to measure the incoming signals. A description of the experimental configuration is given in Annex A.

As both experiments produced comparable results, only the December experiment is described. The complete analysis of the data collected during the first experiment and their comparison to the models are given in [13].

The transmitter was mounted on a 10 m high tower for this experiment. The tower itself was mounted on a 24 m linear rail on the bottom, along which its position could be precisely controlled, in order to acquire data from various source-receiver geometries (Annex A).

The seabed was characterized by a distinct ripple pattern with RMS roughness 1.5 cm, cross-ripple correlation length 25 cm, and skew angle 40° relative to the source-receiver axis.

2.2.1 Temporal signals

Figure 2 gives an example of the signals received by three of the 14 hydrophones, on the same vertical pole.

The nominal critical angle is 28° if the sediment is assumed to have a sound speed of 1720 m/s as measured on the cores. Consequently only the first angle is nominally supercritical, the remaining two angles being subcritical. Although the results do not reflect amplitude variations as automatic scaling applied to each hydrophone, the qualitative differences in the penetration above and below critical are clearly demonstrated, with the subcritical penetration showing a significant decrease in correlation with depth of the hydrophone, suggesting the importance of seabed scattering mechanisms [13].

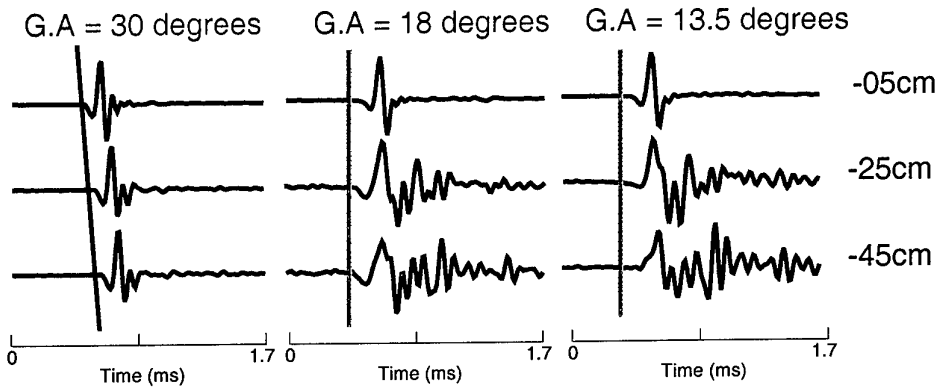

Figure 2 *Examples of signal shapes received on hydrophones 2, 4 and 3 on pole B (see Annex A) for grazing angles* 30°, 18° *and* 13.5°. *Automatic amplitude scaling is applied separately to each hydrophone.*

Above critical angles the three hydrophone signals are highly correlated with a well defined move-out characteristic of supercritical transmission. The signals are virtually replicas of the incident field measured above the interface.

At the two subcritical angles, the received signals have two distinct components. The first part of the signal appears relatively coherent, but with an obvious decrease of high frequency content for increased burial depth. There is no apparent move-out of this arrival with depth, consistent with the prediction of classical transmission theory in the evanescent regime. The second part of these signals appears uncorrelated between receivers and becomes increasingly dominant with depth, consistent with this signal being associated with a seabed scattering mechanism. The dominance of higher frequencies in this part of the signal compared to the initial pulse is also consistent with this interpretation [13].

In conclusion, as emphasized by the red and green lines in Fig. 2, the dominant feature of the signals is the difference in relative arrival time above and below critical angle. Thus, at supercritical angles an increase in delay – or move-out – is observed

with depth. This is consistent with the classical theoretical prediction of the transmitted field propagating downward into the bottom, at these angles [14]. Below critical incidence, classical theory predicts the transmitted field to be a horizontally propagating *lateral wave* with evanescent amplitude distribution in depth. It will therefore manifest itself as having no 'move-out' with depth, a behaviour clearly reflected in the initial coherent component at the two subcritical angles in Fig. 2. This fundamental difference in the temporal characteristics of the penetrated field is a robust indicator of the effective *critical angle* for the sediment, and may therefore be used for estimating sediment sound speed.

Figure 3 gives an example of the amplitude of the signals received by three of the 14 hydrophones on the same vertical pole, for super critical and sub critical insonification.

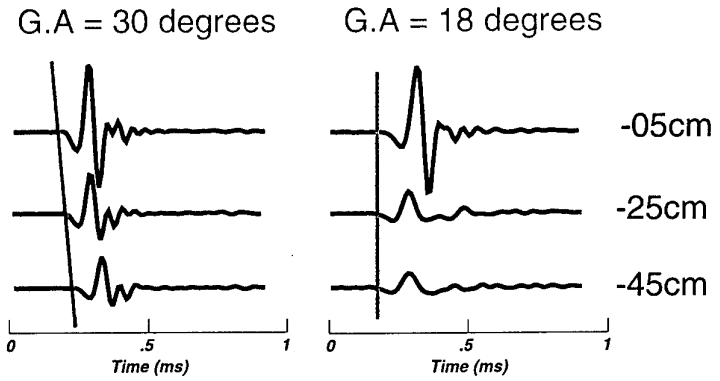

Figure 3 *Examples of signals received on hydrophones 2, 4 and 3 on pole B (see Annex A) for grazing angles* 30° *and* 18°.

The decrease of signal amplitude with grazing angle and burial depth is apparent.

2.2.2 Penetration ratio

To quantify acoustic penetration into sediment, a measure called "penetration ratio" is devised [13]. For a given frequency, the penetration ratio is defined as the magnitude squared of the ratio of the pressure at a point in the sediment to a reference pressure,

$$PR(f,z) = \left| \frac{P(f,z)}{P_{ref}(f)} \right|^2 = \frac{|P(f,z)|^2}{|P_{ref}(f)|^2}. \tag{6}$$

The reference pressure is defined as the pressure amplitude of the incident field at the seabed, i.e. the pressure that would exist at the seabed in the absence of the sediment. Thus, the penetration ratio directly corresponds to the pressure produced

by a unit amplitude incident wave field. To achieve this, the reference pressure is here chosen as the frequency spectrum of the time-gated reference signal (to eliminate the bottom bounce) on the hydrophone in the water (as seen in Annex A). Note that the definition allows the penetration ratio to be larger than unity, or positive in terms of dB, because of the effect of the reflected wave.

Figure 4 shows the estimated penetration ratio in dB at the buried hydrophones on the central pole C (see Annex A), for a series of grazing angles between 13.5° and 30°.

For all three burial depths the highest grazing angle results show a quasi-linear decrease with frequency which is in agreement with Eq. (2) assuming bottom attenuation of $\alpha = 0.5\text{dB}/\lambda$.

At the lowest grazing angles, the penetration ratio is strongly dependent on frequency. For frequencies up to 5-7 kHz the penetration ratio (expressed in dB) decreases quasi-linearly with frequency, the slope increasing with burial depth and grazing angle. As indicated by the dashed lines, this is consistent with the subcritical prediction of classical penetration theory. The lines correspond to the result of Eq. (4) assuming a sound speed of 1626 m/s in the sediment. For the highest frequencies (above 5-7 kHz), the penetration is increasingly characterized by interference fringes as the grazing angle decreases. These interference minima are not located randomly: as the grazing angle decreases, the minima and maxima are shifted down in frequency (for a given burial depth) in accordance with Bragg theory, as the bottom surface contains periodical features.

Quantitatively, it may be observed that the penetration ratio decreases with frequency, grazing angle and burial depth. For example, for the 45 cm hydrophone, losses of 17 dB and 26 dB (compared to the energy that would have been received in the water) are respectively measured at 5 kHz and 10 kHz for a grazing angle of 16°. These values, which represent only one-way transmission loss into the sediment, are very high and imply that the detection of buried mines at low grazing angles will be difficult at these frequencies. Significant energy levels are however penetrating in the bandwidth 2-3 kHz, even at low grazing angles, indicating that this frequency range may be appropriate to the detection of buried objects.

2.2.3 Two-way absorption loss

The sonar equation given in Eq. (1) illustrates the importance of knowing the two-way absorption loss, AL, to derive a buried mine detection system. The 2-way absorption loss into the sediment as a function of grazing angle, frequency and burial depth is computed in this section.

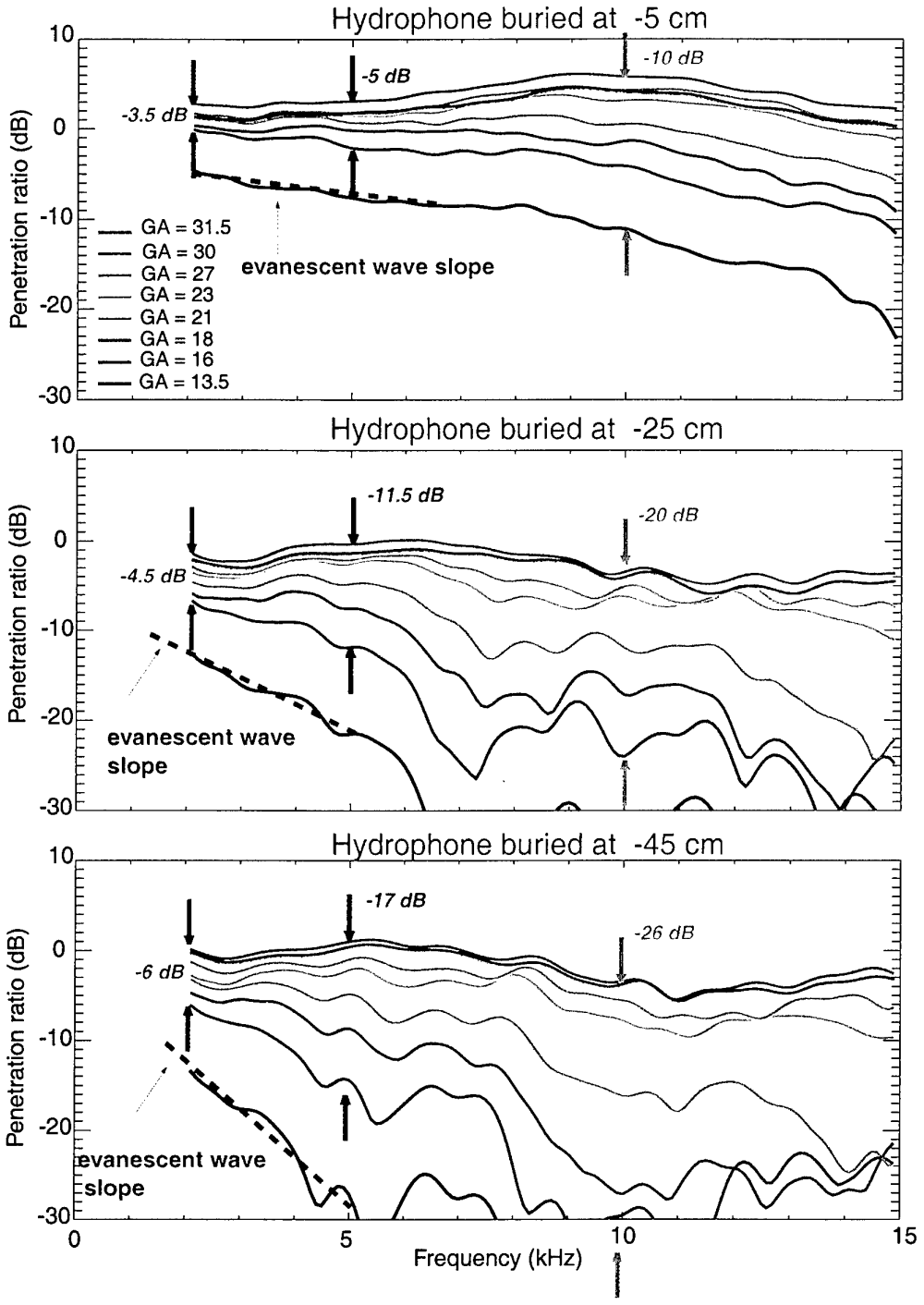

Figure 4 *Penetration ratio in dB versus grazing angles for pole C. Hydrophone 6: burial depth=5cm, Hydrophone 7: burial depth=25cm, Hydrophone 8: burial depth=45cm*

Figure 5 gives the two way absorption loss into the sediment as a function of grazing angle, burial depth and frequency (at 0.5 kHz, 1 kHz, 2 kHz, 5 kHz, 10 kHz and 15 kHz). The curves relative to the frequencies 0.5 kHz and 1 kHz (dashed dotted line) are extrapolated from the data, given that the penetration ratio varies linearly with frequency for a given grazing angle, Eq. (4).

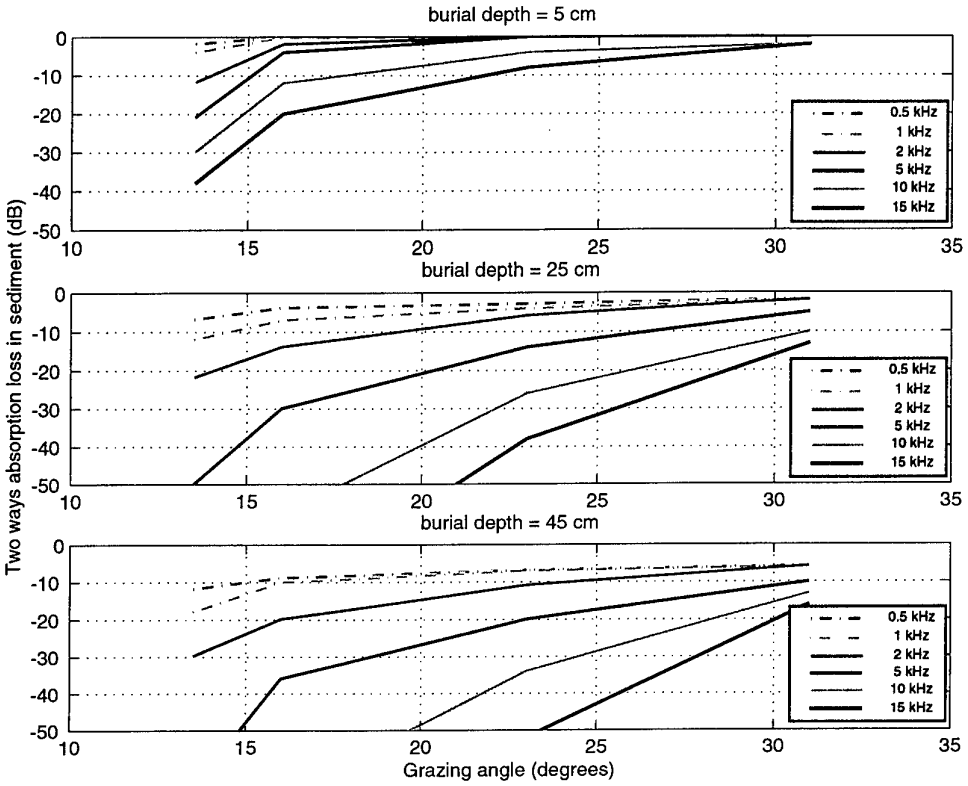

Figure 5 *Two way absorption loss into the sediment as a function of grazing angle, burial depth and frequency. (0.5 kHz, 1 kHz, 2 kHz, 5 kHz, 10 kHz and 15 kHz). The curves (solid line) given for the frequencies 2 to 15 kHz are derived from the data. The curves relative to the frequencies 500 Hz and 1 kHz (dashed dotted line) are extrapolated from the data.*

The absorption loss increases rapidly with burial depth and frequency. Its value remains low only for very low grazing angles and deep burial in the frequency bandwidth 0.5-1 kHz.

2.3 Data-model comparison

The experimental results, from the June 1997 experiment, were compared with two different models (Fig. 6) of the backscatter due to local interface roughness. The first model, OASES-3D [15, 16], uses wavenumber integration in conjunction with a perturbation approach to compute the 3-D coherent and scattered fields in stratified ocean waveguides with rough interface patches. The second model uses Helmholtz-Kirchhoff theory for penetration through a rough surface [17]. The two models used the same synthetic rough surfaces, with spatial characteristics similar to those measured *in situ* by divers during the experiment. Good levels of consistency between the models and the data can be observed. The data suggest that for frequencies below 5-7 kHz, the sound field in the sediment due to subcritical insonification is dominated by the evanescent field, while scattering due to surface roughness is the dominant mechanism for higher frequencies. However, although roughness scattering has been shown to be one mechanism for explaining "anomalous" penetration into sediment, its potential use for detection and classification of buried objects is unclear, considering the low level generated and the possible lack of coherence of the received signals.

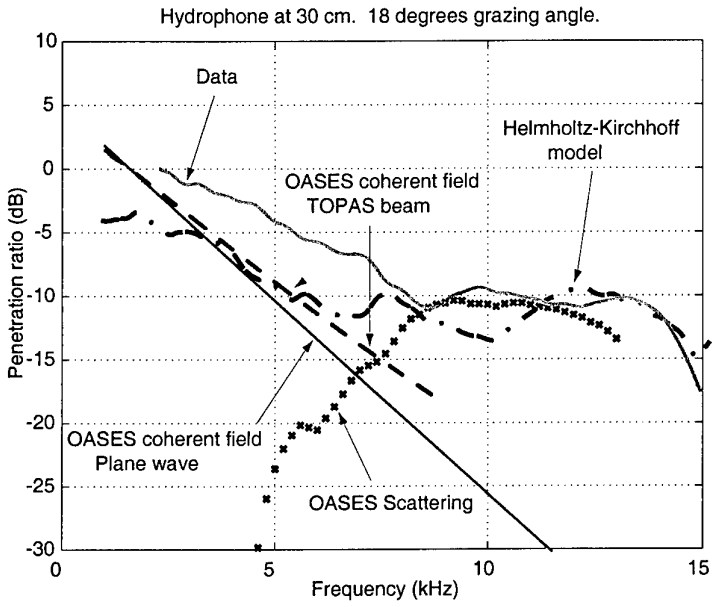

Figure 6 *Measured and modelled penetration ratio for a 30 cm deep buried hydrophone. The grazing angle is* 18° *. Data are shown in green. The OASES coherent field is shown in solid line (plane wave) and dashed line (TOPAS beam). The OASES scattered field is shown by crosses. The Helmholtz-Kirchhoff model results are shown in dashed dot line*

2.4 *Sediment sound speed variation versus frequency*

During the data-model comparison it was found that the frequency dependence of the sound speed in porous sand may have to be accounted for. The data-model comparison yields a sound speed significantly lower that those measured on the cores (1720 m/s at 200 kHz). Simulations using Biot theory [18], which takes into account sediment permeability, have shown that there may be significant frequency dependence of sediment sound speed in the range 1-100 kHz (Fig. 7). The values of the parameters that have been used to compute the curves of the sound speed variation *versus* frequency for different permeabilities of the sediment are given in [19].

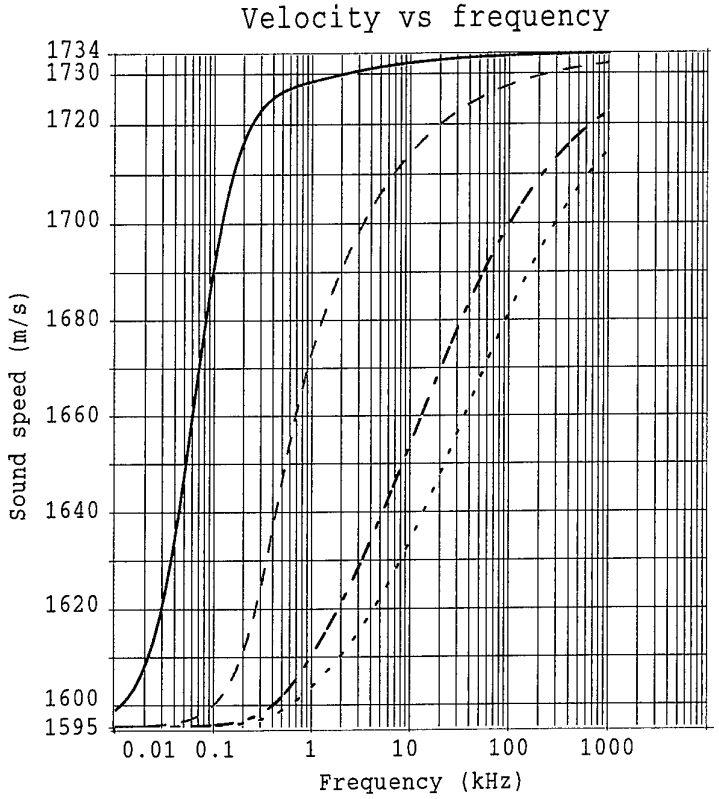

Figure 7 *Sound speed variation versus frequency as a function of bottom permeability obtained from Biot theory. Solid red line: permeability is equal to 1E-09, dashed green line: permeability is equal to 1E-10, dot-dashed blue line: permeability is equal to 1.7E-11 (as measured form the cores taken during the 14-hydrophone array measurements), dotted pink line: permeability is equal to 1E-11*

The variation of sound speed and consequently of the critical angle, as a function of

frequency was therefore investigated [19] by analyzing the variations of signal arrival times *versus* frequency, burial depth, and grazing angle. This inversion method is used in place of the direct estimation of the sound speed derived from the Biot theory which suffers from the complexity of validated measurements of 13 environmental parameters required by the Biot model [19].

The variation of the time of arrival between hydrophones at different burial depths were computed from the acoustic data and compared with the theoretical delays derived from standard reflection theory in discretely layered fluids [2]. The sound speed giving the best match between the measured delays from the *in situ* measurements and the theoretical delays is considered as the sound speed in the sediment where the experiment was performed. Figure 8 shows the best match obtained between the measured delays and the theoretical delays in the frequency bandwidth 2-5 kHz. A very good consistency between the data and the model is obtained for a sound speed of 1626 m/s. A marked discrepancy can be observed between the data and the models for the 1720 m/s sound speed (i.e, the sound speed value measured from the cores).

This value of sound speed in the sandy bottom is quite different to the 1720 m/s sound speed estimated from the cores using pulsed sound at 200 kHz, but is in good agreemeent with the Biot theory prediction shown in Fig. 7. From this figure a sound speed varying from 1600 m/s to 1650 m/s was expected in the bandwidth 2-5 kHz.

The study has demonstrated that, within approximately a frequency decade, the experimental data are adequately modelled by classical theory, provided the *in situ* sound speed estimate is used. This procedure eliminates the need for full Biot modelling with elaborate sediment characterization.

Considering the measured water sound speed of 1515 m/s and the value of 1626 m/s found for the sound speed into the sand, the critical angle is estimated at approximately 21° compared to the 28° critical angle obtained from the cores.

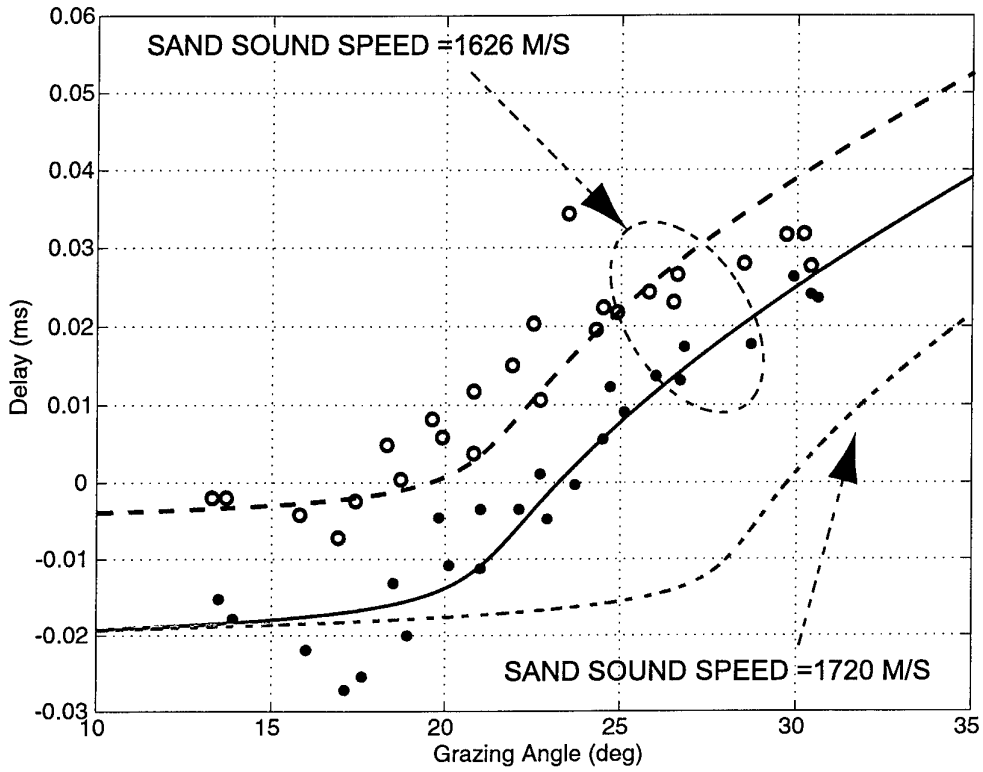

Figure 8 *Sand sound speed estimation from in situ acoustic data analysis. Comparison of measured delays with expected theoretical delays as a function of the grazing angle. Filled and empty circles correspond to the measured delays between hydros at 5 cm and 25 cm and hydros at 5 cm and 45 cm respectively. Red line and dashed blue line represent the corresponding theoretical delays computed from the reflection theory for a sound speed of 1626 m/s between hydros at 5 cm and 25 cm and hydros at 5 cm and 45 cm respectively. Green dotted line represents the corresponding delays between hydrophones at 5 cm and 25 cm for a sound speed of 1720 m/s.*

2.5 Summary

For frequencies below 5-7 kHz, the sediment sound field due to subcritical insonification is dominated by the evanescent field, whereas scattering due to surface roughness is the dominant mechanism for higher frequencies.

Although roughness scattering has been shown to be one mechanism for explaining "anomalous" penetration into sediment, its potential for detection and classification of buried objects is unclear, considering the low level generated and the incoherence of the received signals.

In terms of the hypotheses stated this study concludes:

1. Two different scattering modelling approaches are in reasonable agreement with the penetration observed above 7 kHz, suggesting that the seabed scattering hypothesis is valid at higher frequencies in the bandwidth 2-16 kHz.
2. The finite beamwidth effect is significant at frequencies below 5-7 kHz, i.e, in the regime where direct evanescent coupling is dominant.
3. Although the presence, of a second "slow" compressional Biot wave was not investigated, there was no evidence of the presence of the slow wave in the data. On the other hand, it was found that the Biot theory predicts frequency dependence of the fast wave speed which is qualitatively consistent with the observations.
4. The models account for all the scattering observed, suggesting that volume inhomogeneities are insignificant with regard to penetration in this environment and frequency regime.

Significant levels of energy penetrate in the bandwidth 0.5 kHz –3 kHz, even at low grazing angles. This suggests a potential benefit for using sonars in this frequency range for the detection of buried objects.

Sound speed variation with frequency and concomitant variation of critical angle *versus* frequency, may exist for permeable sandy bottoms, which could hence influence the design of a buried mine sonar.

3

Buried mine detection

The signal-to-noise ratio, introduced in Eq. (1) for a buried mine sonar, depends primarily on bottom backscattering strength, BS, the insonified seabed area, A and the two-way absorption loss into the sediment, AL. Whereas the first two parameters are conventional, valid for any mine detection sonars, the third is specific to the buried mine case.

From a proud mine detection sonar point of view, the insonified area A and the signal-to-noise ratio increased are in inverse proportion, using the highest frequency bandwidth and the highest angular resolution. However, as demonstrated, the penetration of sound into the sediment will be greatly attenuated at the highest frequency. It follows that the advantage of using higher bandwidth to improve signal-to-noise ratio (common with conventional minehunting sonars) will be offset by the corresponding increase of absorption loss. A parametric study is performed at the end of this section to evaluate the performance of a buried mine sonar in regards of this conflict.

The false alarm rate due to bottom reverberation can be reduced by using a system with angular resolution and side-lobe suppression, which will reject environmental backscatter and improve signal-to-reverberation ratio. At low frequency, the necessity for high spatial resolution implies a system with large physical dimensions, difficult to operate using a small towed body or an AUV. The use of parametric sonar was considered as the parametric interaction of two high frequency waves (small transducer) yields difference frequency waves which have the advantage of low frequency and high directivity (that of the primary frequency) with no sidelobes and wide bandwidth [2]. Similarly, synthetic aperture processing achieves high directivity at low frequency with a small antenna, although performance in real conditions, with platform motion, is not well known.

As basic physics of subcritical penetration into sediment were not completely understood, (the term AL was not known), it was not possible to perform a parametric study to evaluate the parameters (transmitting and receiving directivity, bandwidth) necessary for the design of a buried mine sonar. It was therefore decided to use an experimental approach to measure detection capabilities of buried targets at low-

[2]The duality of the high and low frequency could be also used for the discrimination between proud and buried objects

frequency. Several experiments were performed, with different targets and different burial depths, in which backscatter measurements were made on buried objects above and below the nominal critical angle. Target measurements were performed at the same time that measurements on the sound propagation into the sediment were performed.

3.1 Experimental results

3.1.1 Raw data

In order to measure detection capabilities of buried targets in this frequency range, several experiments were performed in which backscatter measurements were made on buried objects above and below the nominal critical angle.

The sonar used was the same TOPAS parametric sonar used for the subcritical penetration measurements. As the sonar generates secondary frequencies in the bandwidth (2-16 kHz), it was not feasible to experimentally investigate the possible gain in detection that could be obtained at low grazing angles while working at lower frequencies (0.5-1 kHz), as suggested by the subcritical penetration results and conclusions from the previous section.

Variation of the signal-to-reverberation ratio as a function of the grazing angle is shown in Fig. 9 for a flush buried 60 cm ϕ solid aluminium sphere. The background levels are estimated by using a standard technique [20, 21].

Above the nominal critical angle, the buried target is detected with a signal-to-reverberation ratio of roughly 25-30 dB. At subcritical angles, detection becomes difficult, although evanescent acoustic waves travel in the sediment below the critical angle, their levels decay exponentially as a function of depth and frequency. Therefore, substantially reduced acoustic energy levels reached the target and were backscattered from it compared with the supcritical angle case.

Other experiments were performed with other types of targets at different burial depths. For example, during the GOATS98 experiment [22], three 1 m ϕ air-filled spheres were buried at 30 cm, flush and half-buried in the sediment. Above critical angle, the detection of the deepest sphere was effective with a loss of 5 to 7 dB in signal-to-reverberation ratio compared to the flush buried target. This loss of signal-to-reverberation ratio between the flush and the completely buried target is in agreement with the absorption loss measured and described in the previous section of this report. The detection of the half-buried target was shown to be effective even at very low grazing angles (15°) with a signal-to-reverberation ratio of the order of 27 dB comparable (only 2 dB loss) to the above critical angle case. This absence of

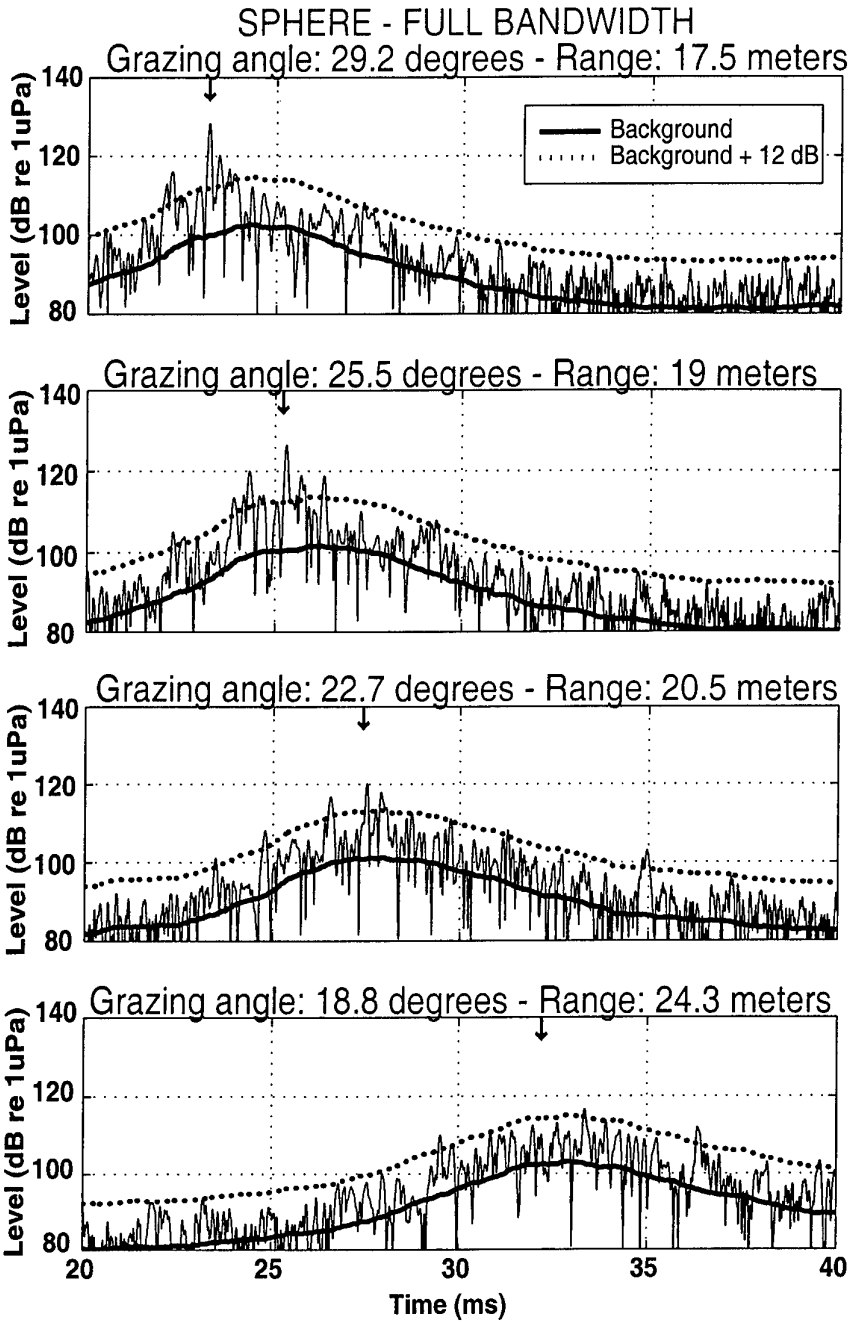

Figure 9 *Variation of the signal-to-reverberation (full bandwidth) for a flush buried sphere as a function of the grazing angle. The solid line is the background estimate. The dotted line is the background estimate + 12 dB line. The red arrow gives the expectation location of the target.*

loss in detection performance observed for the half-buried case at low grazing angles was demonstrated in [1]. The seabed reflected and the direct energy coherently combined to generate a signal stronger than in the free-field case.

3.1.2 Bi-static considerations

In addition to the direct return from the bottom, a strong echo from sea surface reflection, sometimes stronger than the direct return, but fluctuating with sea surface motion, was observed during the experiment while working at low grazing angles. Figure 10 gives an example of the signal received on a 16-element vertical array from the buried sphere.

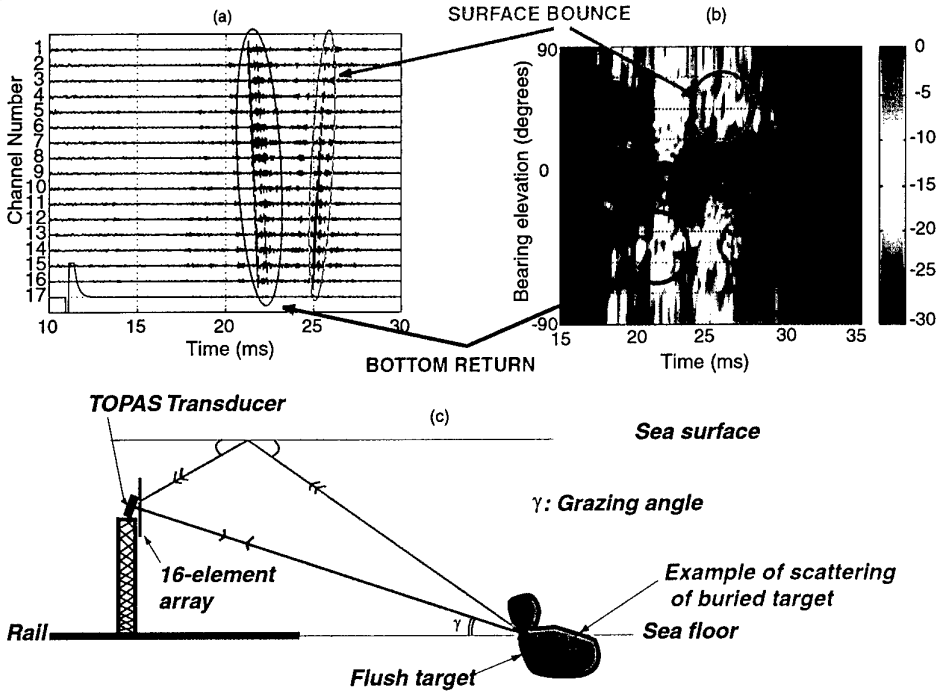

Figure 10 *Direct return and surface bounced return received on a 16-element vertical array from a buried sphere. Figure (a) shows the raw data received on each channel of the array. Figure (b) gives the beamforming output computed from the raw data. Both the direct return (in blue) and the surface bounce (in green) are seen on the plots. Figure (c) shows the spatial backscattering from the target and explains the different paths corresponding to the direct return and the surface bounced return.*

Recent modelling results [1], [23] showed that more energy could be scattered from buried targets, insonified at low grazing angles, in directions closer to the vertical than to the monostatic direction. Whether this energy is received after reflection

from the sea surface in a monostatic configuration or directly in a multistatic mode and the relation of the multistatic echo level to reverberation level are future work items.

Figure 11 shows the variation of the scattering of a flush buried sphere as a function of the grazing angle. For the sphere in the water (red curve), the level of the scattered field oscillates around 0 dB as a consequence of normalization (the scattering strength has been divided by the scattering from a perfect sphere equal to $[a/2]^2$). For the buried target and an incoming wave above critical angle, (green curve), the scattered field has the same amplitude, but the backscattering is confined to angles above the critical angle. For the buried target insonified below critical angle, there is now a scattered field at angles lower than the critical angle, quite low in the backward direction (scattering angles smaller than θ_c on figure) and significantly higher in the forward direction (scattering angles higher than $\pi - \theta_c$ on figure). The maximum scattering is found in a wide angle interval around the vertical direction (scattering angle= 90°), but this field is reduced compared to the other two cases (sphere in water and sphere in sand insonified above critical angle).

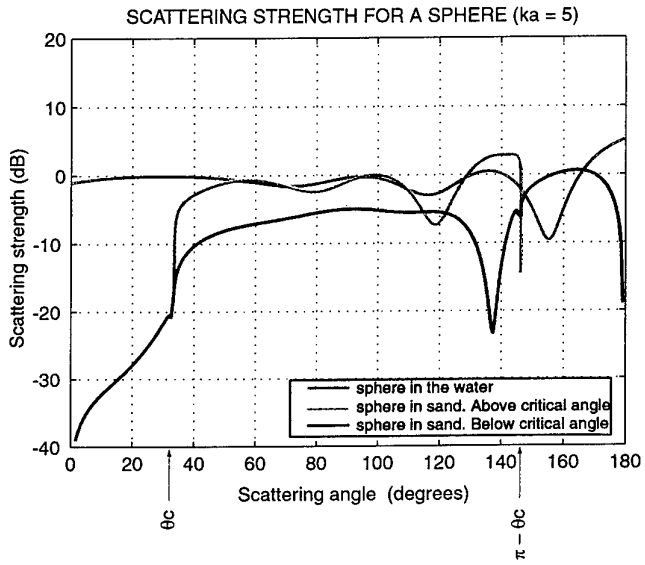

Figure 11 *Scattering from a rigid sphere in water or in sand as a function of the grazing angle. Red curve corresponds to the sphere in water. Green curve corresponds to a sphere in sand with insonification above (35°) critical angle. Blue curve corresponds to a sphere in sand with insonification slighlty below (30°) critical angle. The critical angle θ_c is here* 33.5°.

3.1.3 Physical large array and/or synthetic aperture processing gains

The performance of a detection sonar would be improved by an increase of angular resolution. This effect can be achieved either by using a large receiving physical array (with the drawback of more complex operational use) or by using synthetic aperture processing (with the drawback that the performance evaluation in real conditions is still an issue).

Moreover, as the capability of correctly focusing beams (either real or synthetic) through the sediment for a buried target is still an issue, it was decided to experimentally evaluate the achievable array gain on buried targets [24].

Figure 12 shows the raw data and the synthetic aperture processing results obtained while the TOPAS sonar, moving on a rail, was insonifying a proud sphere and a buried sphere in the frequency range 2-16 kHz.

It is shown that significant improvement in resolution (gain of 8) and signal-to-noise ratio (gain of the order of 8 dB) were obtained, while dealing with buried targets, when integrating successive pings transmitted while the sonar was in motion. By comparison, the gain in signal-to-reverbeartion ratio obtained for the proud sphere is 11 dB. This difference is explained by the difference of synthetic array length which were useful for the proud sphere and the buried sphere. No processing loss seems to be due to the fact that the applied synthetic aperture processing assumes the target in water, neglecting the water-sediment interface and propagation into the sediment.

The synthetic aperture processing results were obtained in ideal conditions, in the sense that a linear trajectory of the sonar existed. Arbitrary sway motion (sinusoidal) was applied to the data to simulate trajectory displacement of the sonar and evaluate the robustness of the synthetic aperture processing at those frequencies. The quality of the output of the synthetic aperture processing was still acceptable up to amplitude sinusoidal variation of $\lambda/8$. This value is quite encouraging and makes the use of synthetic aperture processing feasible at those frequencies. Autofocusing techniques have been proposed to evaluate the platform motion from the data and introduce this estimation of the true trajectory in the synthetic aperture processing [25], [26]. The promising preliminary results make this technique a potential candidate for a buried mine sonar. However additional experiments (GOATS2000) will be carried out in the future to assess operational potential in real conditions.

Similar results were obtained with a physical 12 m linear array [22] which demonstrate the feasibility of focusing through the sediment and the potential of using beamforming techniques to improve the performance of a buried mine sonar.

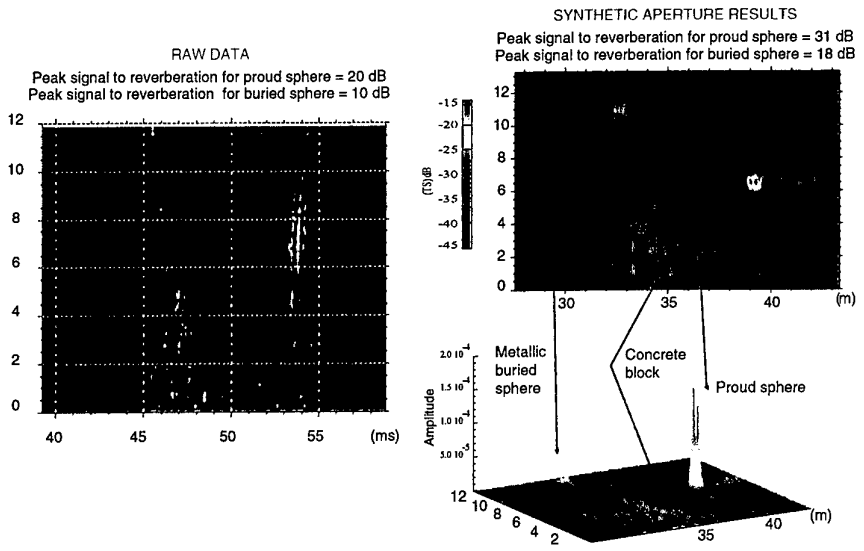

Figure 12 *Raw data and corresponding synthetic aperture sonar results obtained while the parametric sonar was moving on the rail and insonifying both a proud sphere and a buried sphere.*

3.1.4 Matched filter - matched field results

The results presented are the results obtained without a priori information on target and/or noise (ambient noise + bottom reverberation).

The results from subcritical penetration into sediment presented in Section 2 applied to the design a detector which would include the variation of propagation loss into the sediment and therefore the variation of the target echo level *versus* frequency. As the target echo level below the critical angle falls off steeply (assuming evanescent propagation within the sediment as shown in Section 2) with increased frequency, the part of the frequency band where the target echo dominates is retained, whereas the part where reverberation dominates is rejected. The gain in signal to noise ratio is explained by the modelled curves obtained for the target echo levels above and below critical angle and the bottom backscattering shown in Fig. 13.

Figure 14 gives an example of the gain in signal-to-reverberation ratio (of the order of 3-5 dB) below critical angle obtained by emphasizing a relatively narrow band of frequencies at the lower end of the transmitted bandwidth (below 3 kHz).

The size of the insonified "patch" A on the bottom contributing to reverberation is frequency dependent (as decreasing with frequency). Therefore, gain in SNR occurs irrespective of reduced spatial resolution, at lower frequencies.

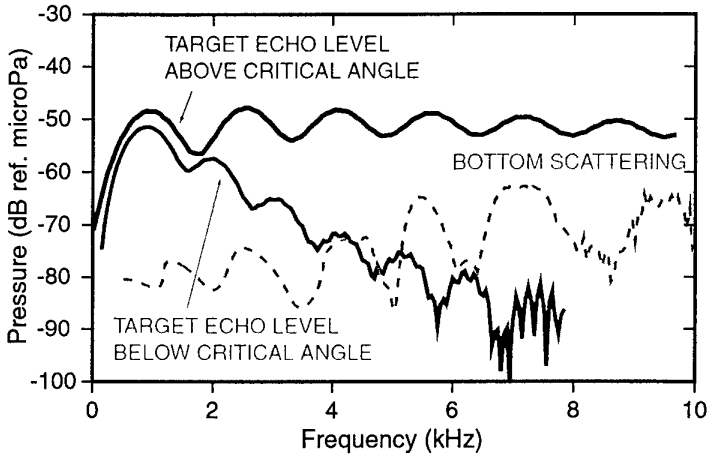

Figure 13 *Relative echo level for a flush buried 60 cm ϕ sphere insonified above (blue curve) and below (red curve) the critical angle as a function of frequency. The bottom backscattering level is shown by the green curve.*

The results of signal-to-reverberation ratio enhancement obtained through low-pass filtering have also been demonstrated by modelling work on the physics of 3D scattering from rippled seabeds and buried targets in shallow water [27]. The gain obtained by limitating the processed bandwidth contrasts with the accepted method of expanding bandwidth to achieve enhanced processing gain against reverberation.

The low-pass filter employed in this example is suboptimal, although it retains some of the characteristics of the target echo. The design of the optimal filter will be highly dependent on bottom characteristics, burial depth of the target to be detected and desired grazing angle. In any case, the gain in signal-to-reverberation ratio gives some level of confidence that robust processing methods can be devised with minimum assumptions regarding target echo structure and noise characteristics.

3.2 Buried mine detection performance system study

Experimental results demonstrated the feasibility of detecting buried mines for grazing angles above and below the nominal critical angle in the frequency bandwidth 2-16 kHz. Above critical angle, detection performance is very high, even for objects buried up to 50 cm into the sediment, but the high grazing angle resuls in reduced area coverage. Below the critical angle, buried mine detection was achieved but with a significantly lower signal-to-noise ratio than for the above-critical-angle case.

The aim of this section is to perform a system study, based on the analysis of the

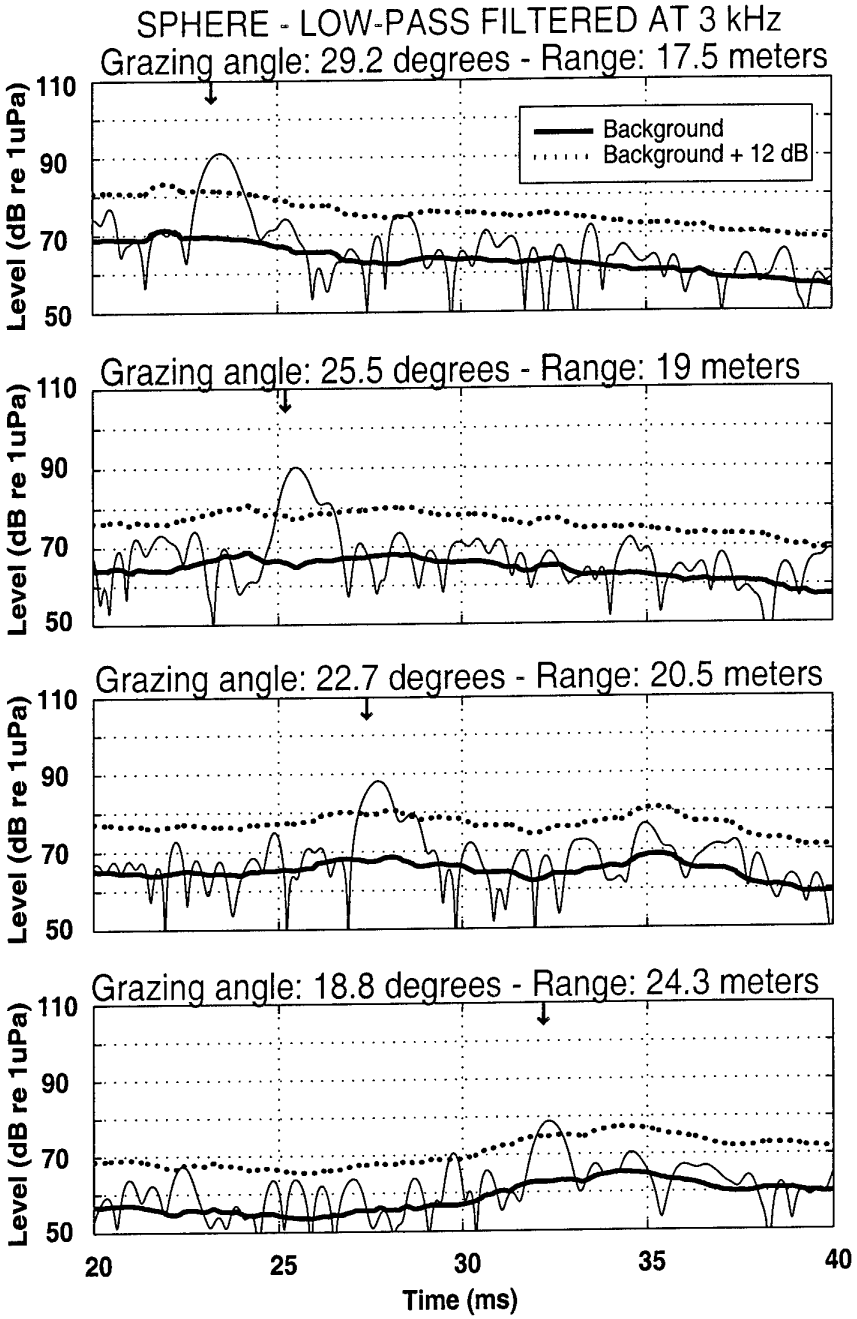

Figure 14 *Variation of the signal-to-reverberation (low-pass filtered at 3 kHz) for a flush buried sphere as a function of grazing angle. The solid line is the background estimate. The dotted line is the background estimate + 12 dB line. The red arrow gives the expectation location of the target.*

collected data, in order to evaluate detection range, as a function of frequency and burial depth.

(1). Variation of the signal-to-reverberation ratio with grazing angle:

The signal-to-reverberation ratios obtained from the data shown in Figs. 9 and 14 are used. Their variation, as a function of the grazing angle, is computed and compared to what should be obtained Eq. (1) and the measured values of two-way absorption loss given in Fig. 5.

For the simulations, it is considered that A, the insonified area, is given by the following expression:

$$A = r\tau\phi c/2, \tag{7}$$

r is the range from the transmitter to the target, τ is the transmitted pulsewidth and ϕ is the -6dB transmit-receive beamwidth.

Considering Eq. 5, the insonified A as a function of the grazing angle is expressed by:

$$A = \frac{H\tau\phi c}{2\tan\theta}. \tag{8}$$

Considering Eqs. (1) and (8), the difference of signal-to-reverberation ratios between two different grazing angles is given by the following expression:

$$SR(\theta_1) - SR(\theta_2) = AL(\theta_1) - AL(\theta_2) - BS(\theta_1) + BS(\theta_2) - 10\log\frac{\tan(\theta_1)}{\tan(\theta_2)}. \tag{9}$$

Assuming Lambert's law variation for the bottom backscattering BS, which was found in agreement with the data, the expression of the bottom backscattering BS can be expressed, for a given frequency, as:

$$BS(\theta) = 10\log\mu + 10\log(\sin^2\theta) \tag{10}$$

Therefore, combining Eqs. (7), (9) and (10) the difference in signal-to-noise ratio can be expressed:

$$SR(\theta_1) - SR(\theta_2) = AL(\theta_1) - AL(\theta_2) - 10\log\frac{\sin 2\theta_1}{\sin 2\theta_2} \qquad (11)$$

From the data shown on Fig. 14, the signal-to-reverberation ratios obtained respectively at 27° and 18.9° are 22 dB and 17 dB in the frequency band 2-3 kHz. From Fig. 5 giving the two-way absorption loss into the sediment, the difference AL(19)-AL(27) is measured equal to -7.5 dB (considering the burial depth of 25 cm for the hydrophone) in the frequency band 2-3 kHz while the last term of the equation is computed equal to 1.2 dB. Therefore, according to Eq. (11) the difference in signal-to-reverberation ratio should be of the order of -7.5 + 1.2 = -6.3 dB, which is in complete agreement with the expected value obtained from the data.

This result is very important in the sense that full agreement is obtained between basic sonar equations and experimental measurements of two-way absorption loss into the sediment and the signal-to-reverberation ratio. The signal-to-reverberation ratio for lower grazing angles can be extrapolated.

Figure 15 summarizes the results obtained for a flush buried sphere and a sphere buried at 15 cm (i.e, the top of the sphere is 15 cm deep) in the sediment. Detection performance of a flush buried 60cm ϕ sphere (having an expected free-field target strength of -16.5 dB) could be achieved at low grazing angles only if array gains are considered. However, the detection at low grazing angles will be difficult in this frequency bandwidth for targets at greater burial depth.

(2). Variation of the signal-to-reverberation ratio with frequency:

As limitations in detection performance at low grazing angles were identified in the 2-3 kHz frequency band, extrapolation of the results to the frequency band 0.5-1 kHz was performed, given the significantly lower two-way absorption loss in that band (Fig.5).

From Eq. (1), the variation of the signal-to-reverberation ratio between two frequencies, for a given grazing angle, may be expressed by:

$$\begin{aligned} SR(f_1) - SR(f_2) &= TS(f_1) - TS(f_2) + AL(f_1) - AL(f_2) - BS(f_1) + BS(f_2) \\ &\quad -10\log\frac{B(f_2)2\theta_3(f_2)}{B(f_1)2\theta_3(f_1))}. \end{aligned} \qquad (12)$$

Assuming as a first approximation that the bottom backscattering was dominated by the surface backscattering (no significant volume scattering) it may be considered that BS varies linearly with frequency. Therefore, assuming a beamwidth varying

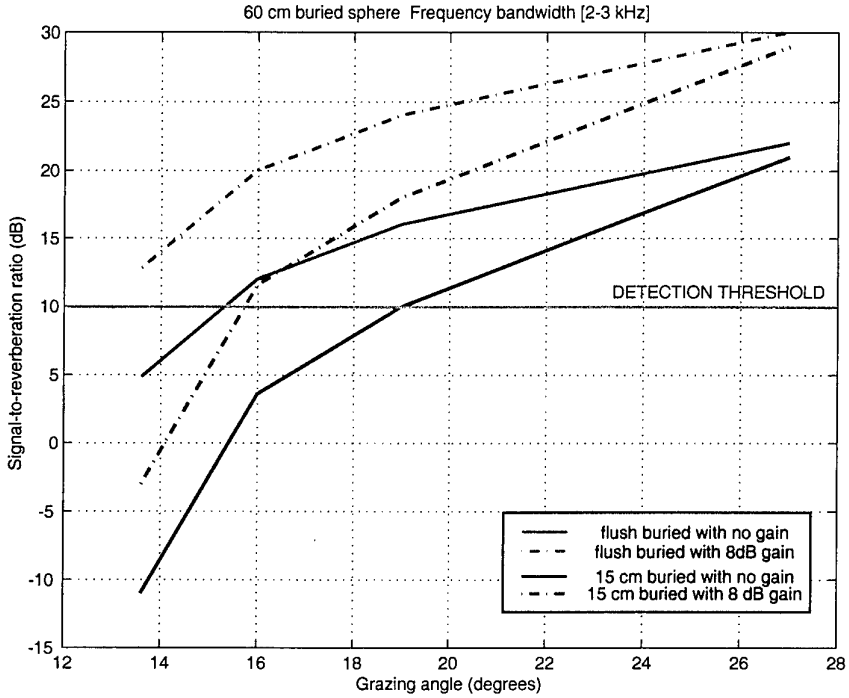

Figure 15 *Variation of the signal-to-reverberation ratio for a 60cm buried sphere as a function of grazing angle in the frequency band 2-3 kHz for two different burial depths (flush or 15 cm buried). The dotted lines are the signal-to-reverberation ratio that could be achieved with a gain of 8 dB expected from larger physical receiving arrays or synthetic aperture processing.*

as the square root of the frequency (for a parametric sonar as described in [28]), Eq. (12) can be written:

$$SR(f_1) - SR(f_2) = TS(f_1) - TS(f_2) + AL(f_1) - AL(f_2) - 10\log\frac{\sqrt{f_2}}{\sqrt{f_1}}. \quad (13)$$

The scattering from a sphere is well known [52, 3] and is dependent on the value of the wavelength λ (or wavenumber k) compared to its radius a. For $ka >> 1$, the behaviour is described as "geometrical" Kirchhoff or "specular" effect. In this case the target strength is independent of the frequency and equal to:

$$TS = 10\log(a^2/4)\ , ka >> 1. \quad (14)$$

For $ka << 1$ the behaviour is described as "Rayleigh scatter" in which the wave diffraction against the body dominates. In this case, the target strength varies as a function of the frequency and is given by the following expression [3] :

$$TS = 10\log(25a^2(ka)^4/36)\ , ka << 1. \quad (15)$$

In the frequency regime 0.5 - 1 kHz considered here, the behaviour of the sphere is more or less in the transition regime as ka varies from 0.6 to 1.2. Therefore, it is difficult to consider the previous equations and a more precise model needs to be used to evalute the change of TS of the sphere between the two bands of interest 0.5-1 kHz and 2-3 kHz. Figure 13 gave the variation of the target echo level as a function of frequency computed from OASES-3D model [15]. From this simulation, a difference of 4 dB in TS for the sphere between the two bandwidths seems to be adequate.

Based on the values obtained in Fig. 5, the signal-to-reverberation can therefore be determined for the 60 cm sphere buried at two different burial depths (flush and 30 cm buried) in the frequency band 0.5-1 kHz. This computation assumes that source level in this frequency band will remain in reverberation-limited conditions.

Figure 16 summarizes the obtained signal-to-reverberation ratio values. Significant gains are achieved at lower frequencies for the lowest grazing angles, allowing the detection of shallow buried targets at low-grazing angles, with sufficiently high ratios. Due to the reduction of the TS of the sphere at low-frequency, the gain is obtained only at the lowest grazing angles whereas a loss in detection performance is observed near critical angle.

It is important to notice that the gain in detection in the 0.5 - 1 kHz range would be lower using a conventional sonar for which the beamwidth varies linearly with frequency instead of the frequency square root.

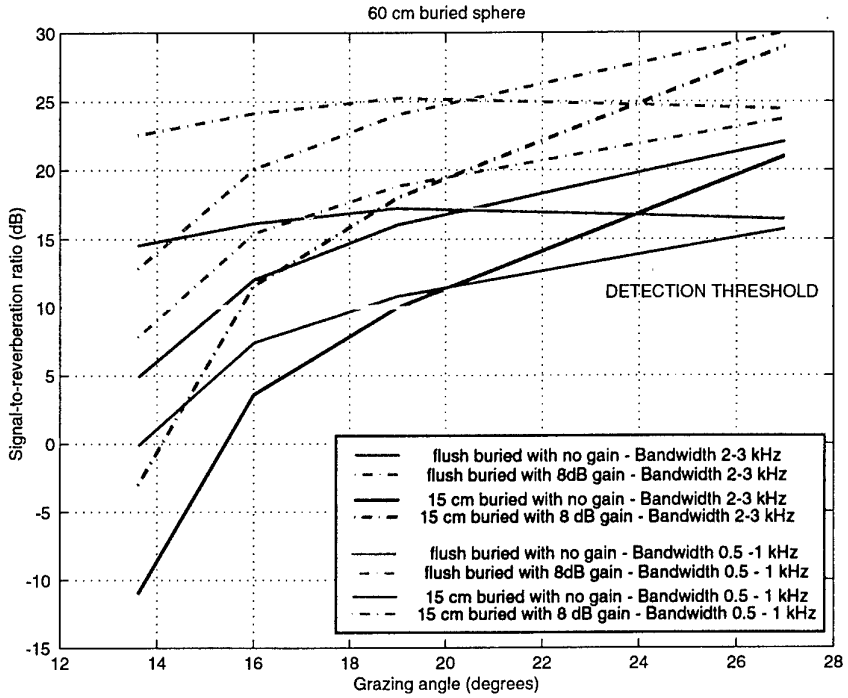

Figure 16 *Variation of the signal-to-reverberation ratio for a 60cm buried sphere as a function of frequency for two different burial depths (flush or 30 cm buried) and two different frequency bandwidths. The dotted lines are the signal-to-reverberation ratio that could be achieved with a gain of 8 dB expected from larger physical receiving arrays or synthetic aperture processing.*

The frequency sensitivity of the signal-to-reverberation ratio has focused on grazing angles lower than the critical angle. It is obvious that in the case of supercritical insonification, the use of lower frequencies will have the opposite effect and lead to a reduction in the signal-to-reverberation ratio.

(3). Variation of the signal-to-reverberation ratio with burial depth:

Considering Eqs. (2) or (4) which show that the penetration ratio varies linearly with burial depth for a given frequency and a given grazing angle, the data have been extrapolated to obtain the two-way loss as a function of the burial depth and

therefore derive the achievable signal-to-reverberation ratios for targets buried at greater burial depths. Figure 17 summarizes the results obtained for 4 different burial depths (flush, 15 cm, 30 cm and 60 cm).

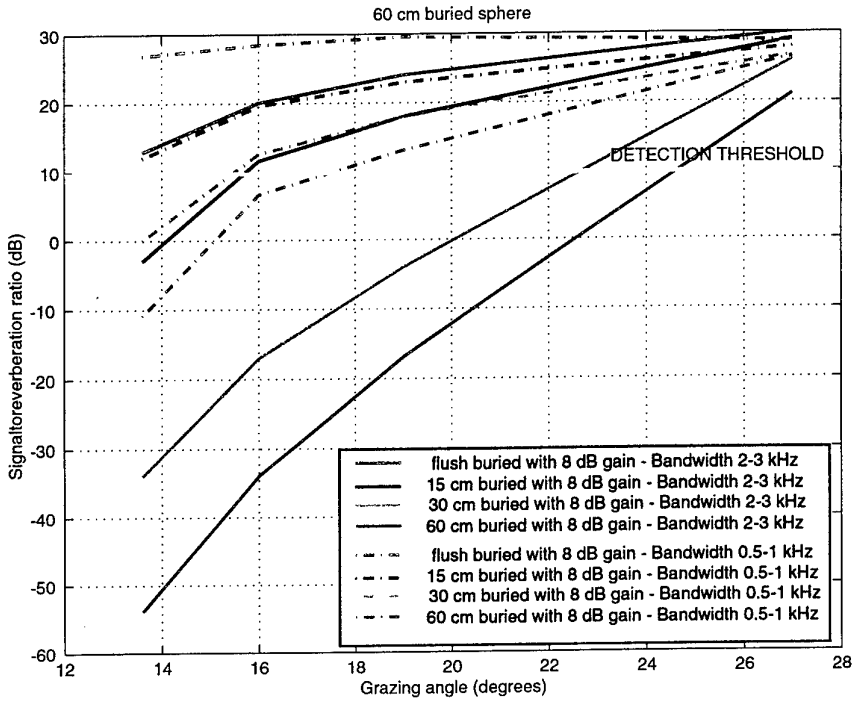

Figure 17 *Variation of the signal-to-reverberation ratio for a 60 cm buried sphere as a function of the burial depth and the grazing angle for two different bands of frequency (2-3 kHz and 0.5-1 kHz). 4 burial depths are considered (flush, 15 cm, 30 cm and 60 cm). The solid lines are the signal-to-reverberation ratios obtained in the frequency band 2-3 kHz. The dotted lines are the signal-to-reverberation ratios obtained in the frequency band 0.5-1 kHz. For all curves a gain of 8 dB expected from larger physical receiving arrays or synthetic aperture processing is considered.*

Detection at low grazing angles will be achieved only for shallow buried targets, even in the low-frequency band 0.5 - 1 kHz.

3.3 Summary

The detection of targets buried in a sandy bottom was found to be effective at above the critical angle, with the operational limitation of reduced area coverage (range equal to 1.75 times the sonar height for a grazing angle of 30° for one side) in shallow water. In order to improve the swept path width, detection performance at low grazing angles was evaluated. Detection at subcritical angles was found difficult.

Significant gains in signal-to-reverberation ratio below critical angle were obtained by emphasizing, a relatively narrow band of frequencies at the lower end of the transmitted bandwidth (below 3 kHz), and by taking into account the quantitative results of the subcritical penetration into the sediment. This effect of enhancing the detection performance of a sonar by limiting the processing is in contrast to traditional sonar technique of expanding bandwidth to achieve enhanced processing gain against reverberation. The design of the optimal filter depends on bottom characteristics, target burial depths and grazing angles.

Significant gains in signal-to-reverberation ratio were also achieved by using either a larger physical array or synthetic array processing. It was demonstrated that focusing of targets through the sediment was possible. No loss of performance was observed to that obtained for a proud target. The synthetic aperture processing results make this technique a potential candidate for a buried mine sonar. Additional experiments (GOATS2000) will be carried to assess operational potential.

Simulation has shown that lower frequencies (of the order of 500 Hz-1 kHz) are mandatory for the detection of buried targets at very low grazing angles and that detection at those frequencies will only be effective for shallow buried targets.

Finally, the detection of half-buried targets was shown to be effective, irrespective of the grazing angles, above and below the critical angle.

4

Target classification and identification

Classification of buried mines and mines in high clutter density areas is an identified operational shortfall. The current approach is based on target echo analysis and when available, the shadow imaged by high resolution, high frequency sonars, which are of limited performance in the case of buried targets and high-clutter density areas. To estimate the potential of alternative classification schemes, the use of sonar systems in the **low-to-intermediate broadband ka range (around 2-40)** was investigated. This approach should allow better penetration into the sediment (buried case) and into elastic targets. Consequently, target backscattering characteristics could be exploited for either proud or buried objects.

To gather more pertinent information from the object echo and therefore to achieve better classification, it was decided to exploit the **aspect dependence** of target backscattering in the frequency band 2-20 kHz. The aspect variation of the target backscattering could for example be acquired by an Autonomous Underwater Vehicle (AUV) circumnavigating the target. The sonar resolution in azimuth is kept coarse enough to ensure, for each ping, complete insonification of the target. In this frequency band, sound waves penetrate the target and the backscattered waves carry information relative to the external shape and the internal properties (material and structure) of the object. Analysis of their variation with aspect and frequency will allow classification as natural or man-made objects and characterization from the estimation of geometrical and elastic properties.

The parallel development of classification techniques and object/waveguide scattering modelling has resulted in **model-based** classification approach.

The development of the proposed **classification and identification** methodology included:

- Preliminary study of the physics of backscattering by simple-shaped objects, such as fluid- (air- or water-) filled, thin-walled cylinders, air-filled thin-walled spherical shells and simulated rocks. Physical interpretation is model-based, deriving from the study of well-proven theories (such as plane-plate theory [29], [30], ray theory [31], resonance scattering theory [32], [33], thin-shell theory[34]) and suitable target scattering simulators [1]. Theoretical investigations of scattering assumed that the targets were in free space, proud on

the seabed and buried in sediment. The experiments were performed first at normal incidence and extended to generally oblique incidence in the case of aspect-dependent shapes.

- On the basis of the physical interpretation, selection of best data representations suitable for outlining discriminating features; selection of features to discriminate among targets, in particular between natural and man-made objects and between objects externally similar but internally different.
- Development of analytical matching models relating the selected features to target parameters of interest for classification/identification purposes.
- Development of model-based classification/identification methodology.
- Validation of physical interpretation using real data from:
  - free-field simple shapes (reference case): air- and water-filled finite cylinders with flat ends;
  - proud simple shapes: the same cylinder used in the free field, filled with water;
  - proud rocks;
  - proud exercise mine (extension of theoretical interpretation on simple objects);
  - buried simple shapes: air-filled spheres.

The analysis of target scattering feature variation (with particular reference to elastic waves) was performed in different environmental conditions, such as presence of boundaries (water-seabed interface), different grazing angles, burial depths, and outer medium geophysical characteristics, etc.

In parallel numerical models were developed for different targets (cylindrical or spherical) in free-field, on the bottom or buried [1]. These models will lead to an understanding of the frequency, temporal and spatial features of the scattered pressure field, which may be exploited for classification purposes, provide information for detection purposes and allow modelling the effects of sediment and the seabed interface on mine scattering characteristics.

4.1 Theoretical concepts of target acoustic scattering at low to intermediate frequencies

At low-to-intermediate frequencies 2-20 kHz the significant contributions to the target echo are not only the specular reflection and potential diffraction effects (significant also at high frequencies), the *background* response, but also the so-called

resonance response, in the case of man-made elastic objects characterized by particular symmetries (e.g., bodies of revolution).

The **background** contributions are related to the external shape of a target, and are returned by any kind of target, whether man-made or natural, impenetrable or elastic. This response component derives from the specular reflection and interaction of diffraction effects from target shape "discontinuities" (such as edges and corners).

The **resonance** component of the acoustic response of an elastic target in the time domain consists of a series of echoes following the specular reflection and in the frequency domain, corresponds to resonance frequency modes, which appear as a combination of dips and peaks. Resonance scattering theory addresses the relation between resonance frequencies and a set of backscattered periodic elastic waves revolving around the target [32]. Every acoustic wave backscattered periodically is assumed to give rise to resonance. Hence, both the helical/circumferential surface waves revolving around the target at its interfaces and the multiple internal bounces, generated if sound can penetrate and propagate inside the object, are included in this definition.

4.1.1 Single-aspect scattering interpretation (normal incidence)

Experiments on elastic wave dynamics were performed initially using fluid-filled thin-walled cylindrical shells with circular cross-section insonified *at broadside* in the free space [35, 36, 37]. The relative thickness, h, defined as the ratio between wall thickness d and outer radius a, is in the range (0-0.3). Figure 18 shows a simplified scheme of travel paths of classes of surface wave families, which revolve around the target cross-section (left) and of multiple internal reflections (right).

The *surface* waves are grouped into: (1) families of shell-borne waves which can be generated by empty or fluid-filled shells, (2) families of outer-fluid-borne waves, some of which are generated only by liquid-filled, thin-walled shells and (3) families of inner-fluid-borne waves, which are characteristic of liquid-filled shells (some types exist only if shells are thin). In Fig. 18, when a wave type is generated also by empty/air-filled shells, then the shell is white inside. In the case of liquid-filled, thin-walled shells, a significant part of the incident sound is assumed to be transmitted into the inner liquid, then reflected several times by the inner shell walls before being partially backscattered [31]. This transmitted component can generate periodical backscattered waves (multiple internal bounces) following either the direct path, or inscripted polygonal paths with even number of sides.

The extent to which the content influences the target response is shown by resonance analysis of simulated data. Figure 19 shows the spectral response and applied resonance identification for an air-filled and a water-filled cylinders of the same size

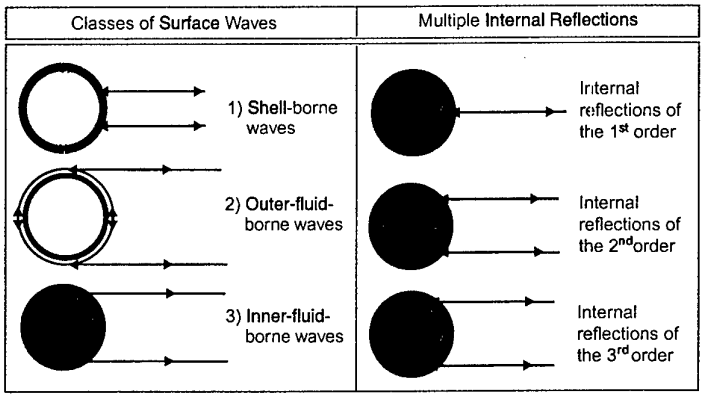

Figure 18 *Main classes of periodical waves contributing to resonance scattering by a thin-walled shell of circular cross-section insonified at broadside.*

and material, at broadside. The water-filled cylinder has a complicated resonance response from which shell-borne, internal-reflection-borne and internal-fluid-borne wave families can be extracted. For the same frequency range, the air-filled cylinder shows the shell-borne wave family only.

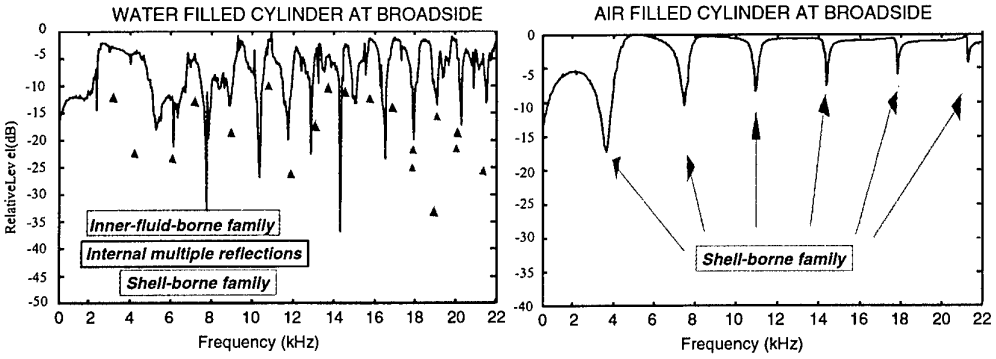

Figure 19 *Comparison of broadside spectral response of two identical cylinders filled with water and air, respectively.*

4.1.2 Multiple aspect scattering

Two cases were considered: a 1 m long solid cylinder with a 50 cm ϕ, and a simulated rock of similar dimensions. The rock was generated using a 3-D fractal algorithm [38]. The algorithm used is a 3-D implementation of the *mid-point displacement* method described in [39].

The acoustic responses of these objects (more precisely, of a horizontal slice of these

objects) was modelled using the time domain finite difference (TDFD) code Robertson *et al.* [40] and implemented in [41].

Figure 20 shows the multiple aspect time and frequency response of the solid cylinder and the rock. Marked differences may be observed between the responses of the two targets.

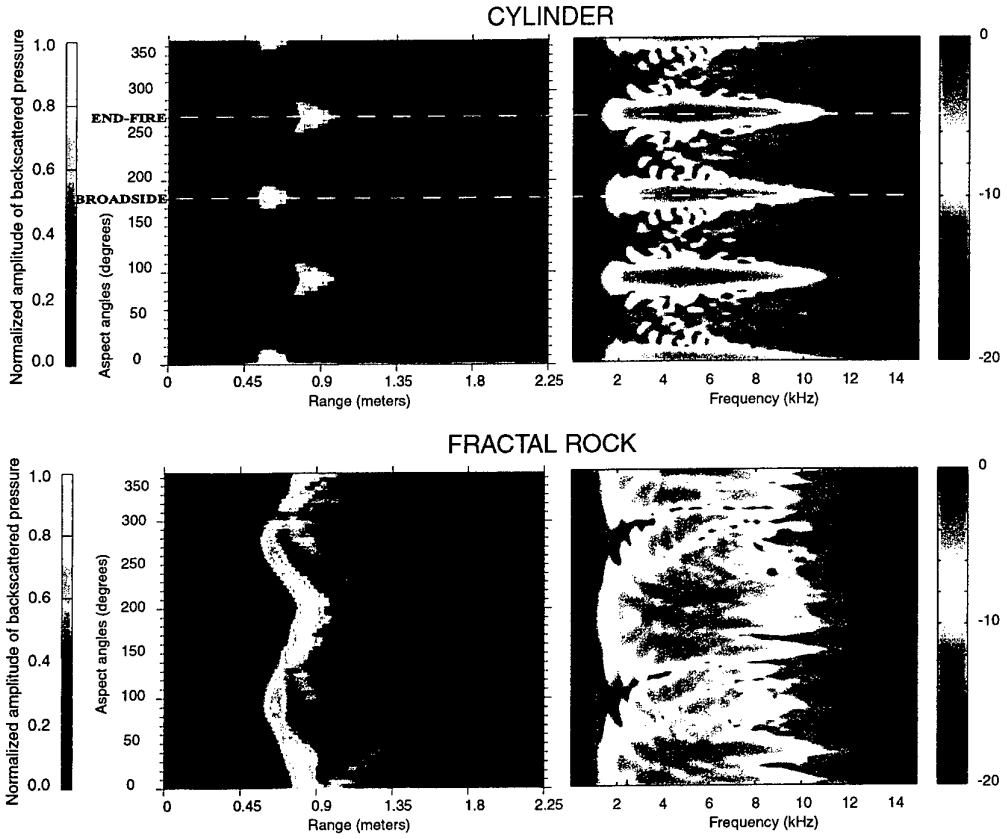

Figure 20 *Modelled multiple-aspect variation of the the time and frequency response of a solid cylinder and a fractal hard rock (2D TDFD simulator). The sampling in aspect angle for the simulations shown is* 5°. *A Ricker 5 kHz (bandwidth 2-10 kHz) is used to insonify the target. The results shown are not deconvolved responses.*

The response of a natural object is dominated by reflection and diffraction effects, which give rise to patterns generally randomly distributed in the time-aspect and frequency-aspect domains. On the contrary, the response of the solid cylinder is characterized in time by quasi-sinusoidal curves and in frequency by quasi-hyperbolic and quasi-parabolic curves, which have symmetries with respect to either broadside or end-fire aspects.

For elastic man-made targets, the analysis considers reflection/diffraction and elastic contributions. Fig. 21 shows the multiple aspect frequency representation of the rigid and elastic features of an air-filled, thin-walled steel cylinder with flat endcaps, obtained from the FEM model of backscattering developed in [1].

From the background response, two families of mode loci, the axial and radial modes, are generated from the interaction of diffraction at the corner (S) respectively with the visible corners (A) and (R), identified in Fig. 21(a). According to the thin-shell theory, generalized in [36] to liquid-filled, thin-walled shells by extending the physical interpretation of elastic phenomena off broadside, the elastic response at low to intermediate frequencies is mainly characterized by helical shell-borne waves (of Lamb-type and shear kinds), outer-fluid borne Scholte-Stoneley waves, inner-fluid-borne surface waves and multiple internal bounces, characterized by helical paths around the shell (Fig. 21(b)).

The diffraction Fig. 21(c) and elastic features Fig. 21(d) appear in the frequency-aspect domain as quasi-hyperbolic and quasi-parabolic symmetry with broadside or end-fire aspects. Hence, they provide regular, patterned textures, which are not evident in the response of natural objects. For an air-filled cylinder, only the helical shell-borne waves (of Lamb-type and shear kinds) not the different families of waves described in the previous paragraph, are shown in Fig. 21(d).

4.2 Classification and identification methodology

Figure 22 summarizes the proposed **classification and identification** methodology. based on multiple-aspect target echo analysis in the time and frequency domains [42],[43].

The multiple aspect response of a target in time and frequency domains *versus* aspect is analyzed in terms of reflection/diffraction features. These features can be processed, for example, by computerized tomography in time and by multi-aspect scattering analysis in frequency. The analysis allows the extraction of information on a target's external shape and approximate size to provide the preliminary classification as natural or man-made.

When the identification of a man-made target is addressed and the target can be assumed as elastic, an approach based on mono-aspect or multi-aspect resonance scattering analysis can be applied. This processing phase is aided by the inversion hints provided by the preliminary classification process in terms of shape and approximate size. It consists of extracting and processing the features from these elastic phenomena generated by the target structure. This information may be able to provide additional target characterization in terms of geometrical and elastic parameter estimates (e.g., more accurate dimension estimates, shell material and thickness, in-

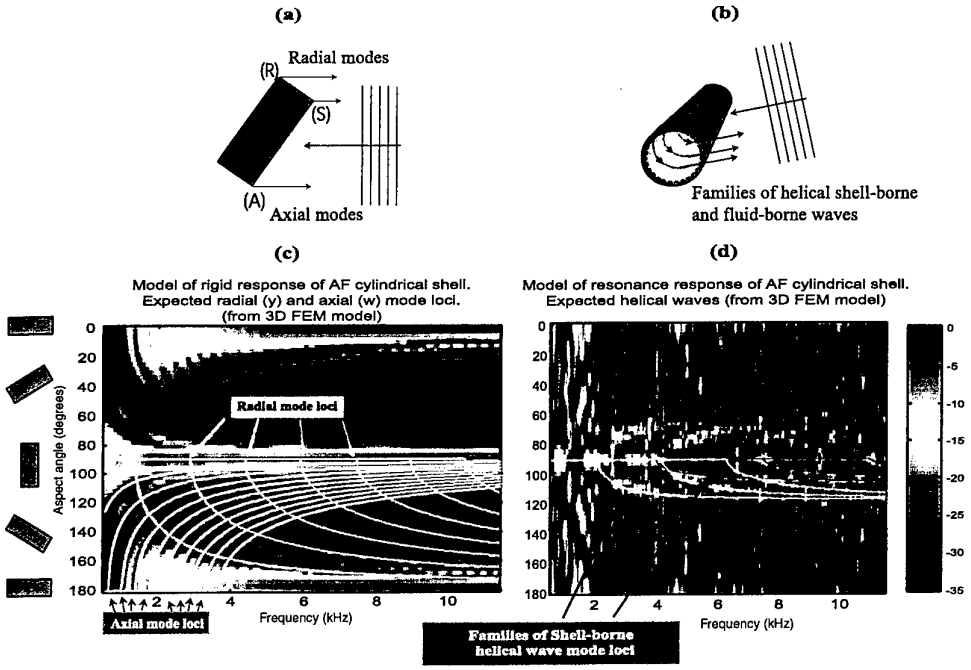

Figure 21 *Simulated background and elastic responses of a steel cylinder with flat endcaps (frequency-aspect domain). Developed models of the diffraction and elastic features are superimposed. Figures (a) and (c) show the two mode loci (radial and axial) from the background response. Figures (b) and (d) show the families of shell-borne helical waves from the elastic response.*

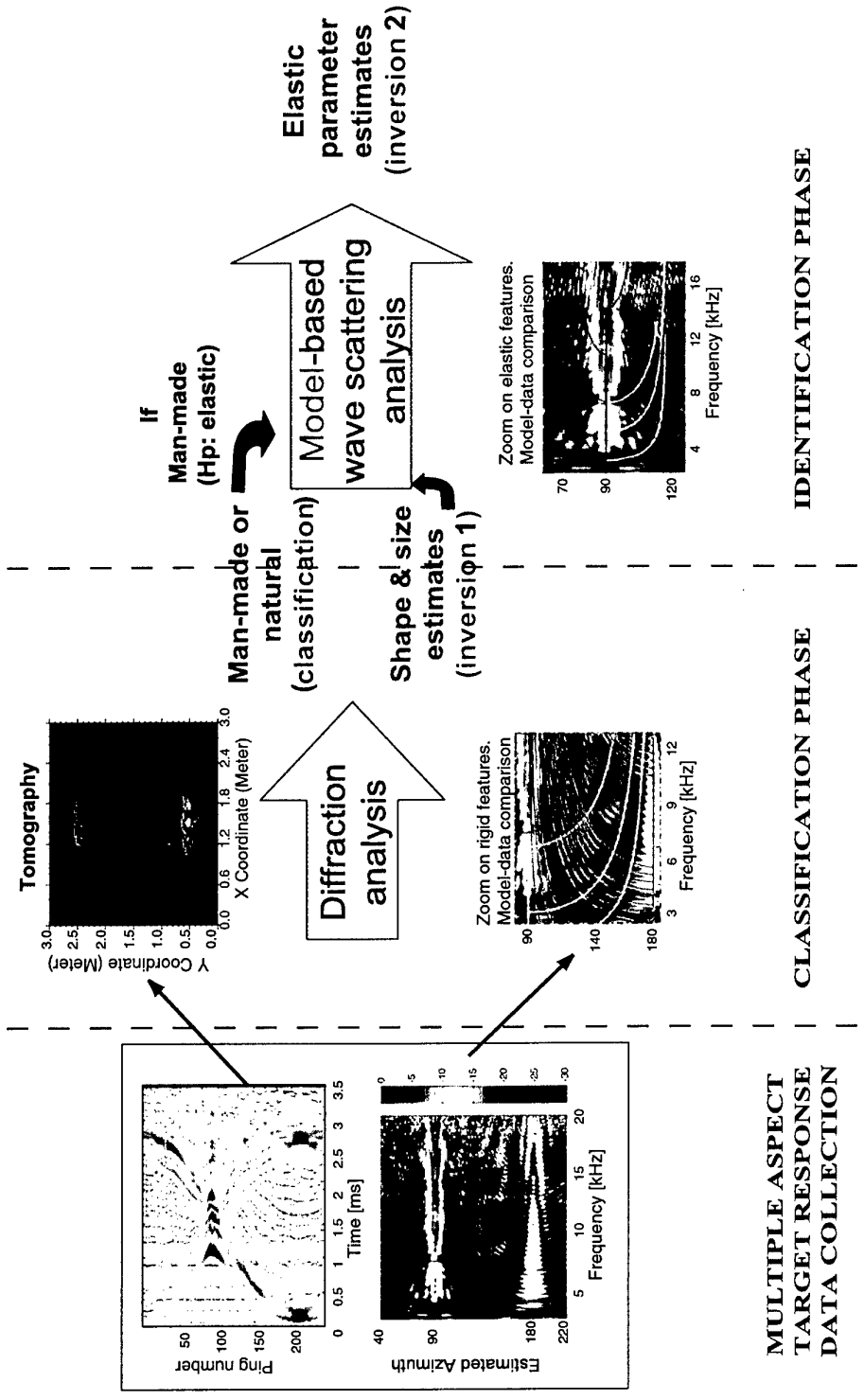

Figure 22 *Schematic of proposed classification-identification methodology*

ner medium properties). This low-frequency approach could allow discrimination between objects of the same external shape with different internal characteristics.

This new multi-aspect broadband classification/identification methodology has been designed for use in conjonction with an AUV circum-navigating the target to acquire the azimuthal variation of the target response. The sonar resolution in azimuth is kept coarse enough to ensure, for each ping, complete insonification of the target. The target aspect resolution is to be kept high enough (typically less than 1^o) to allow one to track the 2D aspect-dependent features in the time and frequency domains.

4.2.1 Classification

The aspect dependence of the echo can be acquired by a sonar mounted on a maneuverable platform circum-navigating the target. This motion corresponds to a 360° azimuth angle variation at constant grazing angle. If the grazing angle is sufficiently low, the approximation can be made that the trajectory of the sonar and the centre of mass of the object are coplanar and thus, simplified 2-D reconstruction methods can be employed. For each acquisition (i.e. each aspect angle) the signal returned can be considered as a projection on the range axis of the reflectivity of the object.

The reflection map of the object is reconstructed from the set of aspect-dependent projections by back-projection. This operation is called reflection tomography [44, 45, 46]. The concept of a target reflection map has been defined previously for a 3-D reconstruction method fusing shadows and echoes from multiple aspects [47].

The potential of reflection tomography is demonstrated on simplified 2-D models. The objects are represented in 2-D by the intersection of their 3-D volume with a horizontal plane passing through their center of gravity.

Figure 23 shows the reconstructed reflection map for the cylinder and the rock obtained from the multiple-aspect temporal representations shown in Fig. 20. The black lines correspond to the contour of the 2-D horizontal cross-sections used in the simulation. The shape and the dimensions of the two objects are clearly shown on the figure.

Although the aspect dependence of backscattering exhibits major differences in the responses of the two objects, the reflection maps give a more immediate understanding of the object geometry.

In parallel to the tomographic reconstruction, the methodology proposes the analysis of the multiple aspect representation in time and/or in frequency for the estimation of the length L and the outer radius a, in the case of an identified cylindrical target.

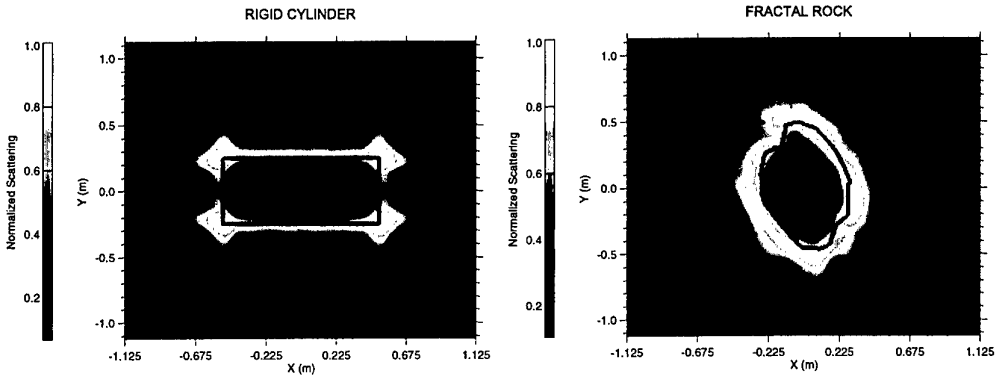

Figure 23 *Tomographic reconstruction of modelled aspect dependent backscattering of rigid cylinder and fractal rock. The modelled data used are those presented in Fig. 20.*

The following table gives the mathematical equations used for the computation of the geometrical parameters.

Diffraction features	Target parameters	Matching model	Applicable to
Axial modes f_n^{Ax}	L	$L = n\frac{c_{out}}{2f_n^{Ax}\sin(\alpha)}$	any cylinder with flat endcaps
Radial modes f_n^{Rad}	a	$a = n\frac{c_{out}}{4f_n^{Rad}\cos(\alpha)}$	any cylinder with flat endcaps

Table 1 *Proposed matching models from thin shell theory for diffraction features*

Here, c_{out} is the outer sound speed around the target, α is the incident angle, n is the mode number.

4.2.2 Identification

If the reconstructed shape of an object is similar to a man-made target shape, it may be assumed that the target is elastic and resonance scattering analysis may be applied in order to further characterize the object in terms of its elastic and geometrical properties.

The physical interpretation of elastic waves dynamics [32, 30, 36] described in Section 4.1 allows us to formulate equations in terms of selected resonance characteristics *versus* target elastic and geometrical properties, e.g. the shell outer and inner radii (a and b respectively), the shell material membrane speed (c^*), and the inner fluid sound speed (c_{in}).

The following table gives the mathematical equations that can be used to estimate the inner radius b (giving, with the known outer radius estimated from the diffraction features the thickness of the shell d), the material sound speed c^* and the inner fluid sound speed c_{in}. In the table c^s denotes for the shear wave sound speed of the shell material and $c^{s/p}$ the shear or compressional sound speed of the shell material.

Elastic waves	Target parameters	Matching model	Applicable to
Lamb S_0 waves $f_n^{S_0}(\|C_{ph,n}\| \rightarrow c^*)$	R, c^*	$(c^* \sin(\alpha)/cout)^2 = 1 - (\frac{nc^*}{2\pi f_n^{S_0} R})^2$	any thin-walled cylinder shell
Shear S waves $f_n^S(\|C_{ph,n}\| \rightarrow c^s)$	R, c^s	$(c^s \sin(\alpha)/cout)^2 = 1 - (\frac{nc^s}{2\pi f_n^S R})^2$	any thin-walled cylinder shell
Inner S_{in} waves $f_n^{S_{in}}(\|C_{ph,n}\| \rightarrow c_{in})$	$b, c_{in}, c^{s/p}$	$1\text{-}(c^{s/p} \sin(\alpha)/cout)^2 = (\frac{nc_{in}}{2\pi f_n^{S_{in}} b})^2$	any thin-walled cylinder shell
$i^{th} - order$ multi-bounce wave r_i	$b, c_{in}, c^{s/p}$	$1\text{-}(c^{s/p} \sin(\alpha)/cout)^2 = (\frac{nc_{in}}{4i \sin(\pi/2i) f_n^{r,i} b})^2$	any thin-walled cylinder shell

Table 2 *Proposed matching models from thin shell theory for elastic features*

At broadside, the analytical matching models for fluid-filled, thin-walled cylindrical and spherical shells are applied by an automatic multi-hypothesis estimation method of resonance analysis. Both the analytical models and the automatic approach of feature extraction/identification and parameter estimation are described in Ref. [36].

4.3 Experimental results

4.3.1 Free-field targets measurements

(1). Reflection map reconstructions

The tomographic reconstruction of the reflection map has been tested on experimental data [48]. The signals backscattered by air-filled and water-filled cylindrical shells 2 m long, 0.5 m ϕ, 6 mm wall thickness were recorded in free-field at an aspect angle variation of approximately 200°. Figure 24 shows the aspect-dependent scattering and the corresponding reflection maps.

As the aspect angle range is 200°, the rectangular horizontal section of the cylinder is only partially reconstructed. However, due to the internal reflection of the back end-cap, a more complete reconstruction is obtained for the water-filled cylinder. Due to the difficulties of rotating the air-filled cylinder (positive buoyancy) at a

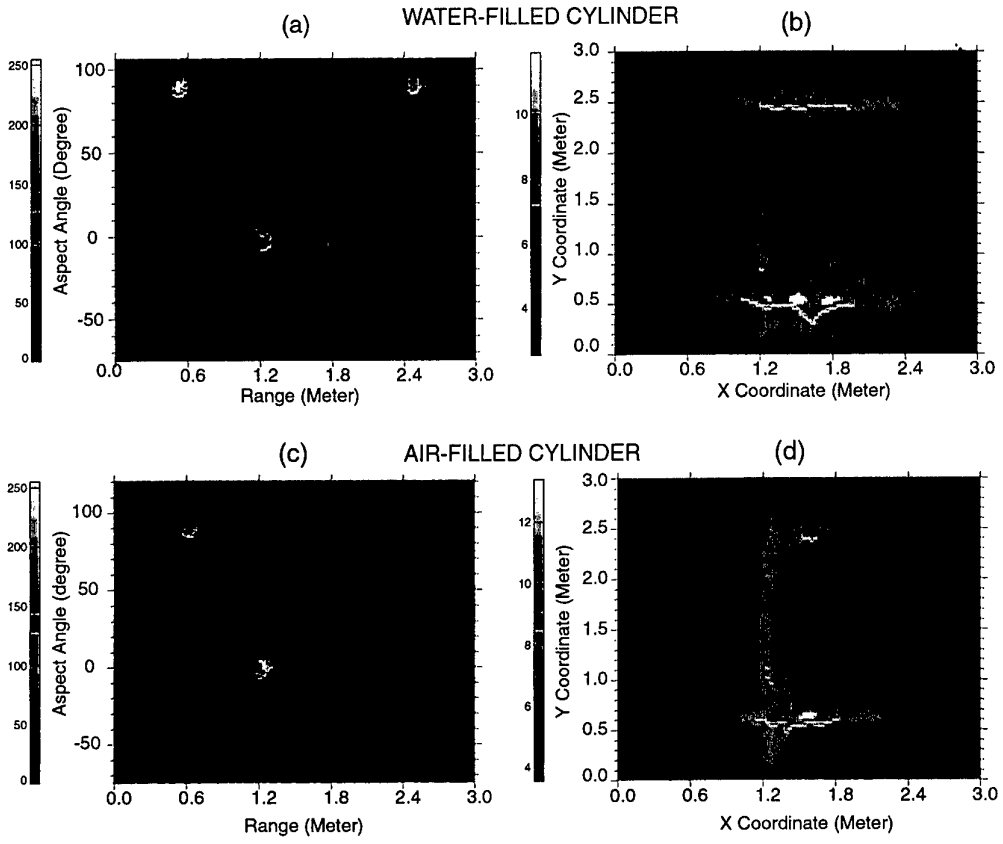

Figure 24 *Tomographic reconstruction of water-filled and air-filled cylinder from multiple aspect data obtained from continuous rotation of the two targets in the free-field. Figures (a) and (c) are amplitude (envelope) of the backscattered pressure for the water-filled cylinder and the air-filled cylinder respectively. Azimuth angle varies from -75 to 120°. Broadside aspect is at 0° e. Figures (b) and (d) are the corresponding reconstructed reflection maps.*

constant speed, its reflection map appears less focused.

For experimental data containing only cylindrical objects, the dimensions and shape were deduced from the high energy areas.

(2). Feature diffraction and resonance scattering analysis in the frequency domain

Figure 25(a) shows the multi-aspect spectral amplitude of the air-filled cylinder the reflection map reconstruction of which was previously computed. The models of a number of mode-loci corresponding to the rigid features (b) and elastic features (c) are superimposed.

Fig. 26 shows the resonance analysis applied to the broadside aspect response of the water and air-filled cylinders. The difference of inner material is evident from the different spectral responses.

The values of the target parameters seen in Table 3 from the automatic multi-hypothesis estimation method described in [36] are in good agreement with the expected values. Table 3 shows the estimation of four target parameters (outer radius, shell thickness, inner fluid speed, shell material speed) without using the information contained in the reconstructed reflection map. The introduction of the object shape and approximate dimensions in the estimation process allows one to reduce the space of solutions for the unknown parameters, leading to more accurate and reliable estimates.

Target Property	Input Value Range		AF Shell Estimate		WF Shell Estimate		Expected Value
	No size hint	Size hint	No size hint	Size hint	No size hint	Size hint	
a (cm)	[10,50]	[20,30]	17.5	24.6	37.5	25.6	25
d (mm)	[3,50]		5.3	5.3	8.2	4.1	6
c_{in} (m/s) (WF only)	[900,2000]				1487	1546	1527 (WF)
c^* (m/s)	[3500,5600]		5095	5275	5270	5465	5435

Table 3 *Inversion results from data scattered by a steel cylindrical shell filled with air (AF) and with water (WF). Resonance analysis at broadside, either aided or not by tomographical reconstruction.*

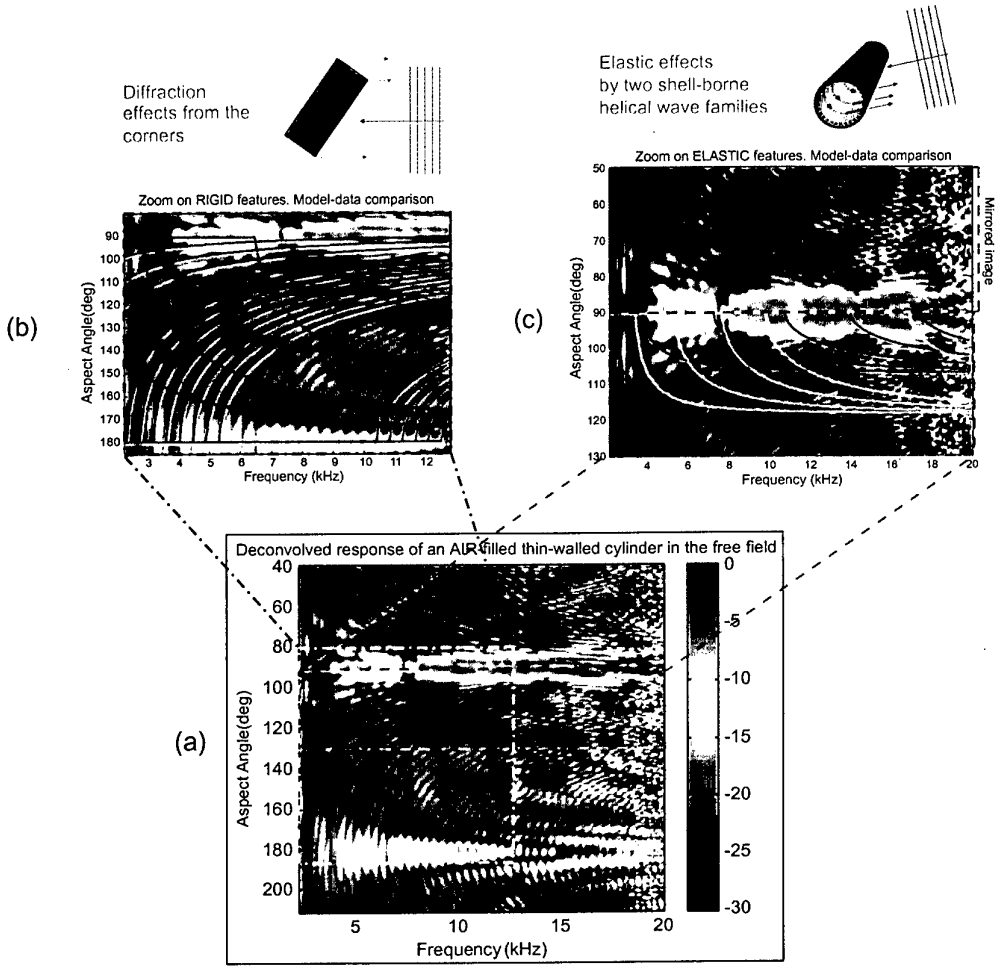

Figure 25 *Multi-aspect amplitude spectrum variation of an air-filled cylinder recorded at sea. Model-data comparison of the rigid and elastic features. (a) Total multi-aspect response, (b) Zoom on rigid features. Data model comparison. (c) Zoom on elastic features. Data model comparison. The red and blue curves in (b) correspond to axial and radial modes respectively. The black and white curves in (c) model S_0 Lamb-type and shear shell-borne wave modes respectively.*

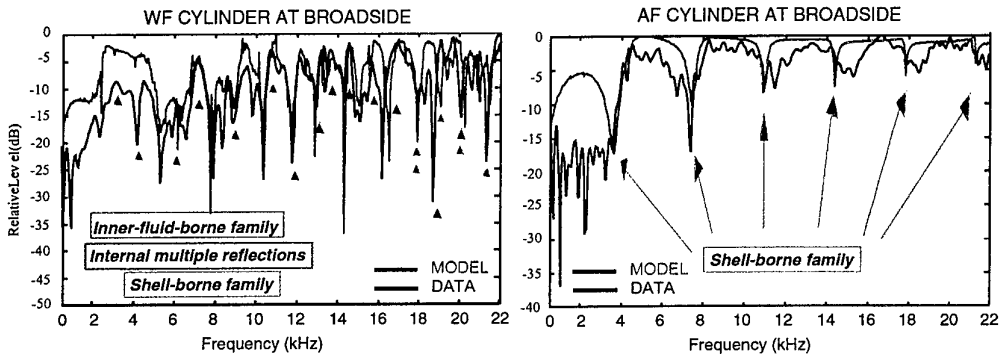

Figure 26 *Resonance analysis of air-filled cylinder and water-filled cylinder while insonified at broadside. Data are in black. Model is in blue*

4.3.2 Proud target measurements

Figure 27 shows the first attempt to discriminate between man-made targets and natural objects. A comparison of the multi-aspect spectral representation, obtained at sea, from a cylindrical exercise mine and a rock on the seabed, is given. The data were collected with the portable underwater rail designed at SACLANTCEN, used in static conditions. The comparison of real data shows the same kind of energy distributions outlined by comparing simulated data (Fig. 20). The response of the exercise mine is characterized by geometric patterns distributed according to symmetries with respect to certain axes. The rock shows randomly distributed patches of energy.

The multiple aspect spectral representation of the cylindrical exercise mine (Fig. 28) shows diffraction (Fig.28a) and elastic features (Fig. 28b). The preliminary analysis of resonance scattering contributions provides the identification of modes of shear and S_0 Lamb-type waves, the dynamics of which are related to the target radius and shell material.

If the diffraction analysis in Fig. 28a is compared with the interpretation of simulated data from a cylinder with flat endcaps (Fig. 21c), each axial mode locus corresponds to one dip curve, whereas for the exercise mine, the modelled axial mode loci overlap alternatively dip and peak curves of the response. This effect might derive from the shape of the target, which has one flat endcap and one other partially oblique endcap. The resulting smoother shape of this latter endcap should give rise to a more limited diffraction effect. According to this interpretation the resulting diffraction pattern characterizes this exercise mine type and hence can be considered part of its signature.

Multi-aspect frequency analysis was applied to the water-filled cylindrical shell in

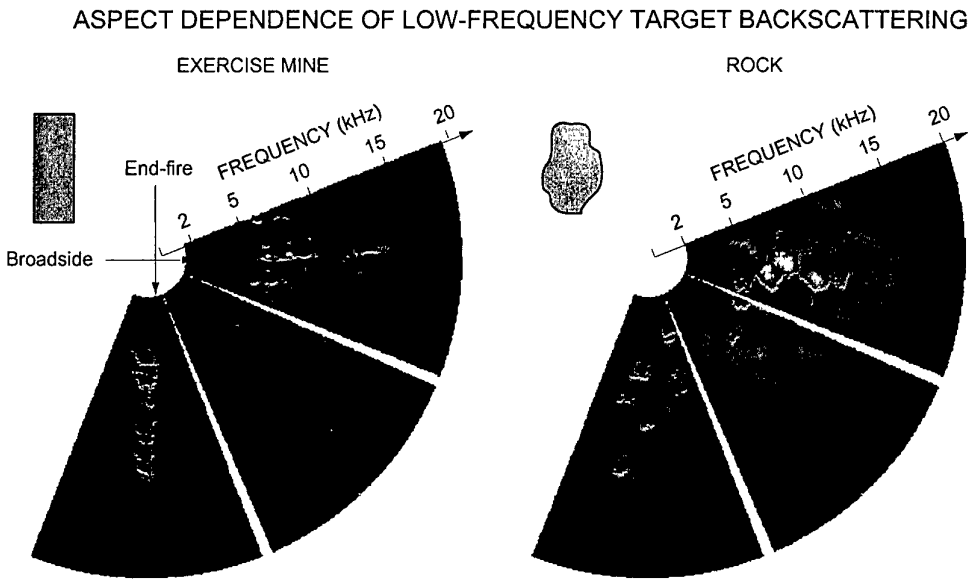

Figure 27 *Comparison of spectral amplitude variation with aspect of an exercise cylindrical mine and a natural rock from real data recorded at sea.*

the free-field. A comparison between free-field (Fig. 29a) and bottom response (Fig. 29b) revealed that elastic features are evident in both cases, some of which were matched by corresponding computed models. At the selected low grazing angle (11°), the elastic behaviour is similar, and hence not significantly influenced by the bottom boundary. [36]

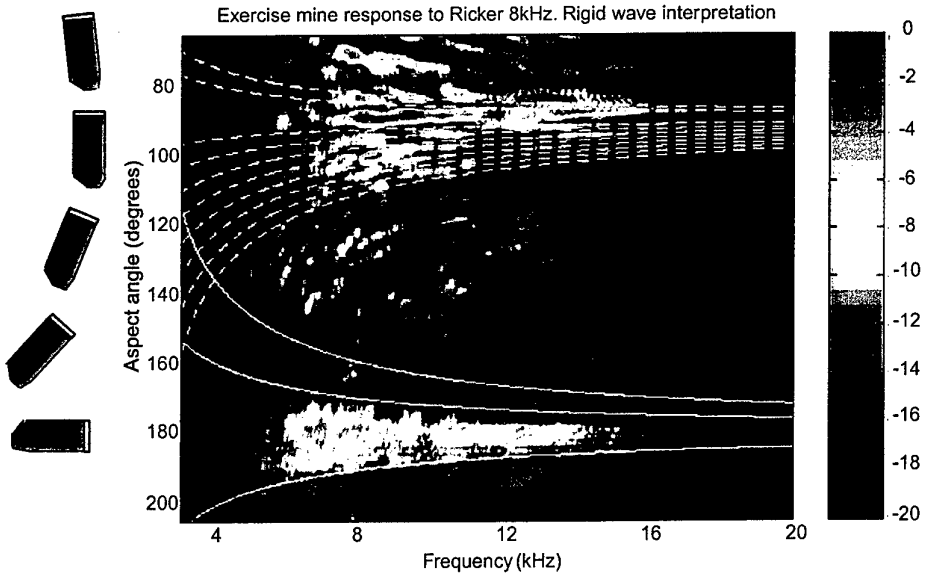

(a)

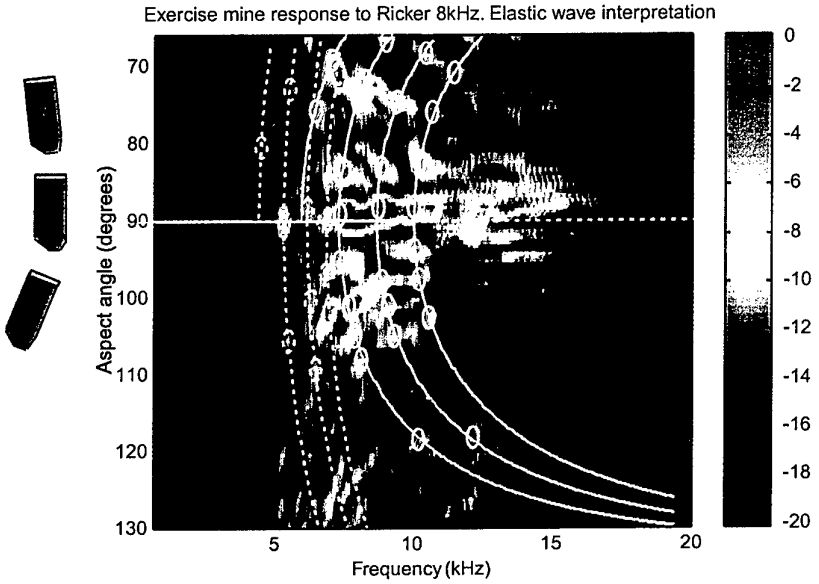

(b)

Figure 28 *Rigid and elastic feature identification of MP80 exercise mine laying on the bottom. The dashed lines in (a) correspond to the modelled axial mode loci, the solid lines to the radial mode loci. The preliminary analysis of resonance scattering contributions in (b) provides the identification of modes of shear (dotted curve) and S_0 Lamb-type waves (solid curve). The dotted and solid curves were obtained by connecting energy peaks (outlined by circles) generated at the intersection of the elastic wave modes with the diffraction mode loci.*

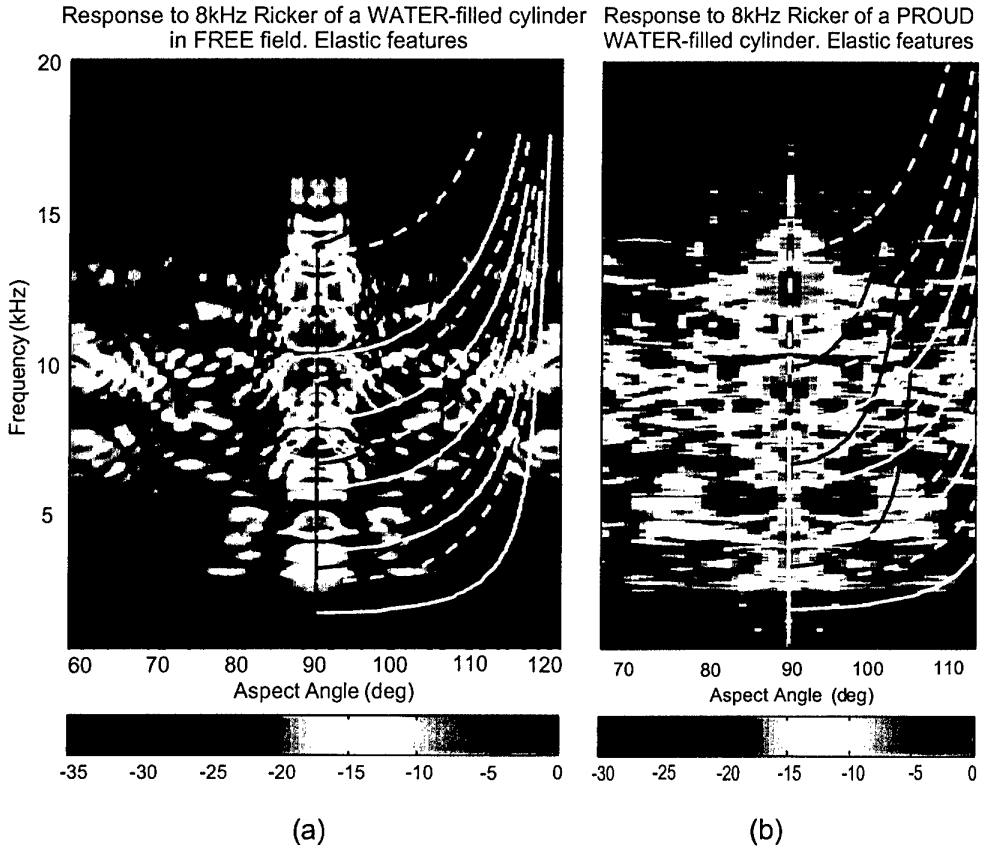

Figure 29 *Comparison of multi-aspect spectral response of a water-filled cylinder in the free-field (a) and proud on a sandy bottom (b). Zoom around broadside aspect. Focus on elastic feature identification (black: S_0 Lamb-type; white solid: shell-borne shear; white dashed: inner-fluid borne shear waves)*

4.3.3 Buried target measurements

Scattering measurements and modelling were used to establish whether circumferential waves (used for the resonance analysis) backscattered by an elastic axisymmetric target in the free space, remain detectable and identifiable when the target is buried [49, 50]. The target was an air-filled sphere, characterized by a limited number of families of resonance waves in the free-space, measured in the free-field, half-buried or flush buried in a sandy bottom [22].

In the selected frequency range, two wave families are outlined as the most significant: the symmetric S_0 Lamb-type waves and the A Scholte-Stoneley (creeping) waves. The response of the sphere suspended in mid-water is presented in Fig. 30(a), where comparison with the computed model is outlined. Model-data agreement is good in feature identification, but poor in level prediction, at late time. Indeed, a decay of about 5 dB of the measured mid-frequency enhancement is estimated with respect to expectation. This mismatch is evident also in the time domain in correspondence with the Scholte-Stoneley wave echoes. It may derive from potential non-uniformity of the sphere wall thickness and/or from the presence of a steel ring attached to the top of the sphere.

The response of the flush-buried sphere is plotted in Fig. 30(b). Both the wave families outlined in free-field data are evident and their scattering levels relative to the specular echo are comparable with the free-field (FF) case.

The dispersion curves of the S_0 and A waves estimated in the free-field (FF), half-buried (HB) and flush-buried (HB) cases are compared in Fig. 31. The S_0 Lamb-type waves are shell-borne and supersonic travelling with phase and group speeds asymptotically tending to the shell material membrane speed, c^*. The A Scholte-Stoneley waves are outer-fluid-borne, subsonic and have the phase speed tending to the outer medium sound speed, the group speed reaching its maximum at the coincidence frequency, f_c, i.e., the frequency at which this family is coupled in phase with the A_0 antisymmetric Lamb-type wave. Their dynamics, as burial depth changes, is predictable.

The first 3 modes (but particularly the first one) of the S_0 wave shift down in frequencies with burial depth, which is a predictable inertial loading phenomenon [51]. For higher frequencies, the expected higher dispersion due to the sediment is negligible, all three curves almost coincide and tend to c^*_{steel}, as expected.

In accordance with theory, the phase and group speeds of the A waves tend to increase with burial depth (i.e., with the average speed of the outer media in which this wave travels) and frequency. The mid-frequency enhancement region shifts up with burial, together with the coincidence frequency, which, for steel, is linearly related to the average outer-medium sound speed [49].

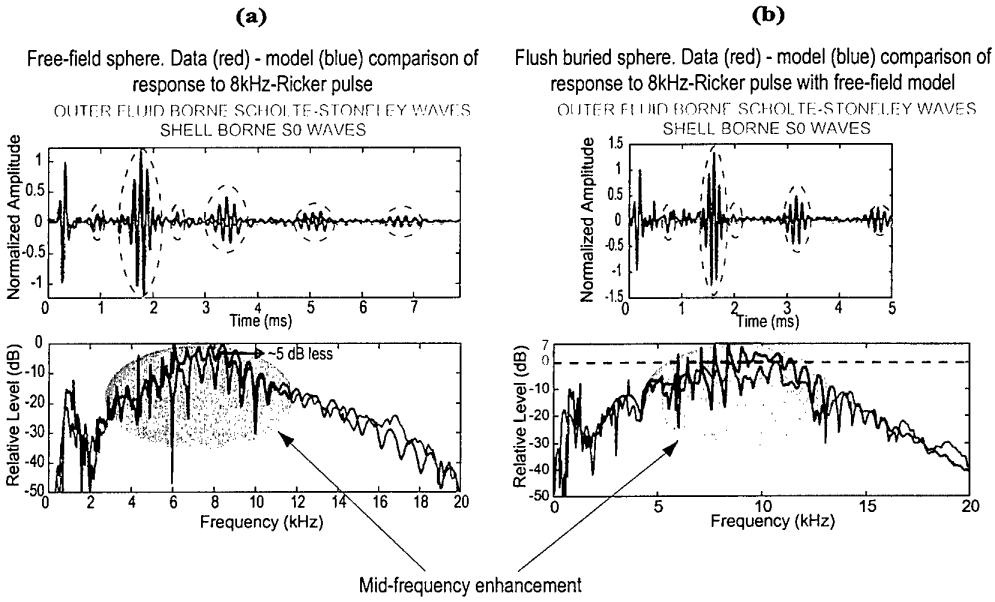

Figure 30 *Data-model comparison of the time and frequency response of a 1 meter ϕ sphere in the free-field (a) and flush buried (b). The model used assumes the sphere is in free-spaceeven while considering the flush-buried case.*

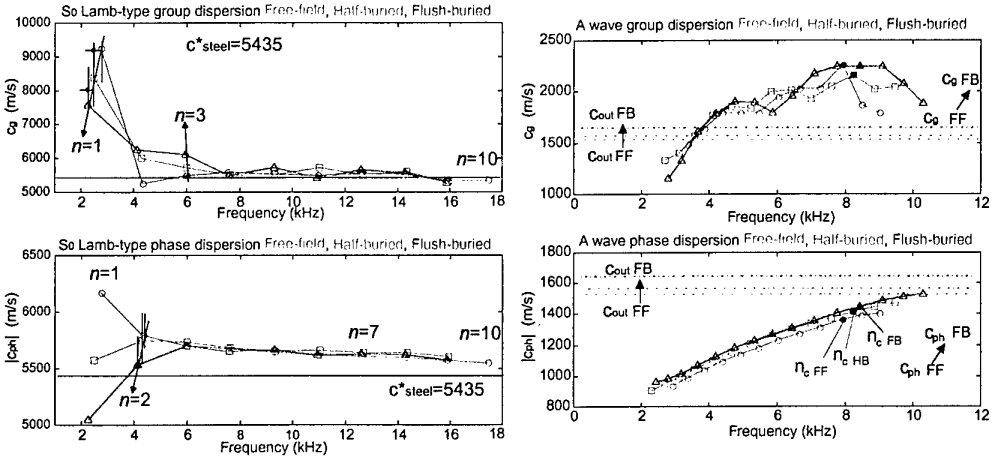

Figure 31 *Comparison of dispersion curves of the S_0 and A waves estimated for the 1 m ϕ sphere measured in the free-field, half-buried and flush-buried.*

4.4 Summary

A method based on multiple-aspect target echo analysis in time and frequency domains, which considers the rigid response (returned by any kind of target) and the so-called resonance response (in the case of man made objects having particular symmetries) was presented.

The potential of the method to discrimate between man-made targets (exercise mine, cylindrical targets) and natural objects (e.g rocks of similar sizes) was demonstrated in simulation and on real data acquired at sea. Geometrical and elastic parameters (material, thickness) were estimated, through resonance scattering analysis, for simple-shape cylindrical targets. The approach, which was developed and validated on free-field data from simple-shape targets, provided good results on the same targets proud on a sandy bottom. Rigid and elastic features were detected and identified for an exercise mine laying on the bottom. The proposed classification approach could be used to complement high-frequency minehunting classification techniques for proud mines.

The existence of resonance waves was also shown on experimental data for a buried sphere. Elastic wave dynamics were computed and interpreted on the basis of recent theories. The amplitude levels of the resonance waves were comparable, relative to the specular echo between the free-field and the buried case, which makes the low-frequency classification methodology applicable also to buried objects.

5

Conclusion and future work

We believe that we have been able to resolve the very important issue of the mechanisms contributing to subcritical penetration into the sediment. The evanescent wave is dominant at the lower frequencies 2-5 kHz of our band of interest 2-16 kHz whereas roughness scattering dominates at the higher frequencies (above 5 kHz for our bottom type). However, although roughness scattering has been shown to be one mechanism for explaining *"anomalous"* penetration into sediment, its potential for detection and classification of buried objects is unclear because of the low level and the lack of coherence of the received signals. In addition, significant amounts of energy penetrate into the sediment in the bandwidth 0.5-3 kHz, even at low grazing angles. This suggests a potential benefit from using sonars in this frequency range for the detection of buried objects. It was demonstrated that sound speed variation with frequency, and therefore variation of the critical angle versus frequency, could exist in permeable sandy bottoms, a fact which has implications for the design of a buried mine sonar.

The detection of buried targets was found to be effective at above critical angle. At subcritical angles, detection becomes difficult. Significant gains in signal-to-reverberation ratio below critical angle were obtained either by emphasizing a relatively narrow band of frequencies at the lower range of the transmitted bandwidth (below 3 kHz) or by using a larger physical arrays or synthetic array processing to improve sonar resolution. No loss of performance, compared to the proud case, was observed when applying array processing (synthetic or real aperture) to buried targets. The results obtained with the synthetic aperture processing make this technique a potential candidate for buried mine sonar. Additional experiments will be carried out in the future to assess operational potential. Despite these gains, preliminary simulation has shown that lower frequencies (of the order of 0.5-1 kHz) are mandatory for the detection of buried targets at very low grazing angles and that detection at those frequencies will be effective only for very shallow buried targets.

A classification/identification method is described based on the multiple-aspect target echo analysis in the time and the frequency domains, which considers the rigid response (returned by any kind of target) and the so-called resonance response (in the case of man made objects having particular symmetries). The classification result is obtained on the basis of estimation of external shape and internal target properties. Its potential was demonstrated by simulation and with real data (exer-

cise mine, cylinders and rocks) for proud targets. Encouraging preliminary results were also obtained for buried spheres. This method could be used to complement current classification techniques for classifying proud targets which have similar external shapes, or as a main classification tool when current techniques fail (e.g, for buried targets).

Future work will be dedicated to the validation of the results presented here on more complex cases (different bottom type, different targets) through modelling and at-sea experiments, in order to be able to specify a system design for the detection and the classification of buried mines.

From a detection point of view, a more exhaustive parametric study will be performed to estimate the optimal parameters (central frequency, frequency bandwidth, directivity) of buried mine detection sonar. This study will be influenced by operational constraints, in terms of acceptable coverage rate and maximum search depth of buried targets. The conclusions about the optimal system design will change considerably as a function of these parameters. Particular attention will be given to the bottom reverberation modelling. In this report, the bottom backscattering was considered to be generated mainly by surface backscattering. However, the structure of the underlying seabed lends itself to producing sediment volume scattering the effect of which will be higher at lower frequencies due to the increased acoustic penetration. The effect of volume scattering on the the buried mine sonar performance will be quantified. The effect of seabed roughness on surface scattering will be quantified as a function of frequency and grazing angle in order to be able to incorporate the information in the sonar equation. The significant decrease of the bottom backscattering at lower frequencies for insonification along the ripple direction will be experimentally validated.

Future classification work will focus on the application of the proposed approach to the classification of different types of mines and objects and the validation of the above promising preliminary results. As reliable target classification techniques require accurate models, the realism of the acoustic target signature will be increased by migrating from 2-D to 3-D modelling techniques. Extensive modelling of more complex targets will be used to interpret and validate experimental data. The robustness of the selected classification approach will also be investigated for limited signal-to-reverberation ratio target responses and for partail and completely buried targets. The influence of bottom interface generating interference null in the spectral response (proud targets) and the influence of bottom roughness (buried targets) will be also investigated.

Finally, Automatic procedures of feature extraction and identification in multi-aspect scattering analysis will be investigated.

6
Acknowledgments

Collaborations with Henrik Schmidt from MIT (on sabbatical at the Centre for one year) and John Fawcett for the targets modelling and Eric Pouliquen for the sound penetration modelling contributed greatly to the success of this work. Through this collaboration, it was demonstrated that the Centre is a unique place representing both system and environmental expertise and that joint effort between the two is necessary and compulsory to achieve substantial scientific results.

The authors would like to thank the Engineering Technology Department which did a great job, not only during but prior the cruises. We would like particularly to thank: Piero Guerrini, Head of the departement Per Arne Sletner who, as Engineering coordinator, succeeded in assembling different systems (acoustics, mechanics and electronics) which functioned during all the cruises, Alberto Figoli for setting up the 16-hydrophone array and hydrophones and the data acquisition electronics, Roberto Chiarabini for assuring the good functioning of the TOPAS system, and Marco Paoli and Marco Tavernelli for mechanical work. We would like to express our gratitude to Lavinio Gualdesi and Umberto Cortis for their contributions to the design and the realization of the TOPAS rail facility. This rail facility was essential to the success of the experiments, as it allows controlled accurate measurements. Enzo Michelozzi for the boomer survey, the sidescan survey and not least, his enthusiasm and advices.

The authors would like to thank Marco Mazzi, from the Mine Countermeasures Group, who was ADP (acquisition and data processing) coordinator for all the cruises and their preparation. His skills and motivation were always greatly appreciated and played an important role in the very high quality of the collected data. Massimo De Grandi who helped him in his task has also to be acknowledged.

We would like to thank the Manning crew (Pino Spairani, Giuliano Bertoli and Giovanni Cuiffardi) for their help and their constant availability during the experiments.

We would like to thank T.Lyons who made his digital close-range stereo photogrammetry system available for the experiments and allowed precise measurements of the bottom spectrum.

The diving team (Marco Paoli, Alessandro Brogini, Lavinio Gualdesi and John Staveley) and divers from a company in Elba was essential for the optimum location

and deployment of all the rail, targets, hydrophones and cables.

Many thanks to the Italian Navy that provided its tank facilities for conducting experiments and reference targets.

Finally, many thanks to the reviewers of this report who, thanks to their pertinent remarks, definitely increased its quality and readability.

References

references in TOC (DAA, 2/97)

[1] Fawcett, J., Summary of object/waveguide scattering modeling at Saclantcen (1995-1998). SACLANTCEN SR 298, La Spezia, Italy, SACLANT Undersea Research Centre, 1998.

[2] Brekhovskikh, L. M., *Waves in Layered Media.* New York: Academic Press, second ed., 1980.

[3] Clay, C. S. and Medwin, H. *Acoustical Oceanography: Principles and Applications*, ch. 10, appendix 10. New York: Wiley, 1970.

[4] Lopes, J. L., Observations of anomalous acoustic penetration into sediment at shallow grazing angles, *Journal of the Acoustical Society of America*, 99, 1996: 2473-2474, (Abstract).

[5] Chotiros, N. P., Mautner, A. M., Løvik, A., Kristensen, Å., and Bergem, O. Acoustic penetration of a silty sand sediment in the 1–10-kHz band, *IEEE Journal of Oceanic Engineering*, 22, 1997: 604-615.

[6] Thorsos, E. I., Jackson, D. R., Moe, J. E., and Williams, K. L. Modeling of subcritical penetration into sediments due to interface roughness, in *High Frequency Acoustics in Shallow Water* (Pace, N. G., Pouliquen, E., Bergem, O. and Lyons, A. P. eds.), SACLANTCEN CP-45, 563-569, NATO SACLANT Undersea Research Centre, 1997.

[7] Jensen, F. B. and Schmidt, H. Subcritical penetration of narrow Gaussian beams into sediment, *Journal of the Acoustical Society of America*, 82, 1987:574-579.

[8] Chotiros, N. P. Biot model of sound penetration in water saturated sand, *Journal of the Acoustical Society of America*, 97, 1995: 199-214.

[9] Jackson, D. R., Briggs, K. B., Williams, K. L. and Richardson, M. D. Tests of models for high-frequency seafloor backscatter," *IEEE Journal of Oceanic Engineering*, 21, 1996:458-470.

[10] Ivakin, A. N. and Lysanov, Y. P. Theory of underwater sound scattering by random inhomogeneities of the bottom, *Soviet Physics Acoustics*, 27, 1981: 61-64.

[11] Hines, P. C. Theoretical model of acoustic backscattering from a smooth seabed, *Journal of the Acoustical Society of America*, 88, 1990:325-334.

[12] Lyons,A. L., Anderson, A. L. and Dwan, F. S., Acoustic scattering from the sea floor: Modeling and data comparison, *Journal of the Acoustical Society of America*, 95, 1994: 2441-2451.

[13] Maguer, A., Bovio, E., Fox, W. L. J., Pouliquen, E., Schmidt, H. Mechanisms for subcritical penetration into a sandy bottom: Experimental and modelling results, SACLANTCEN SR 287, La Spezia, Italy, SACLANT Undersea Research Centre, 1998.

[14] Jensen, F. B., Kuperman, W. A., Porter, M. B. and Schmidt, H. *Computational Ocean Acoustics.* New York: AIP Press, 1994.

[15] Schmidt, H., Lee, J., Fan, H. and LePage, K., Multistatic bottom reverberation in shallow water, in *High Frequency Acoustics in Shallow Water* (Pace, N. G., Pouliquen, E., Bergem, O. and Lyons, A. P. eds.), SACLANTCEN CP-45, 475-481, NATO SACLANT Undersea Research Centre, 1997.

[16] Schmidt, H. *OASES: Version 2.1. User Guide and Reference Manual.* Massachusetts Institute of Technology, 1997.

[17] Pouliquen, E., Lyons, A. P., Pace, N. G. Penetration of acoustic waves into sandy seafloor at low grazing angles: The Helmholtz-Kirchhoff approach, SACLANTCEN SM 290, La Spezia, Italy, SACLANT Undersea Research Centre, 1998.

[18] R. B. Stoll, *Sediment Acoustics*, Springer-Verlag, New-York, 1989

[19] Maguer, A., Fox, W. L. J., Schmidt, H and Bovio, E. Sediment sound speed and critical angle estimations derived from in situ acoustic measurements. Submitted to Journal of the Acoustical Society of America. SACLANTCEN SR 297, La Spezia, Italy, SACLANT Undersea Research Centre, 1999.

[20] Fox, W.L.J., Maguer, A. Detection of buried objects at low grazing angles: Preliminary experimental results. SACLANTCEN SR 293, La Spezia, Italy, SACLANT Undersea Research Centre, 1998.

[21] Bendat, J.S, Piersol, A.G. *Engineering Applications of Correlation and Spectral Analysis.* New York: John Wiley and Sons, 1980.

[22] Schmidt, H., Maguer, A., Bovio, E., Fox, W.L.J, LePage, K., Pace, N.G., Guerrini, P., Sletner, P.A, Michelozzi, E., Moran, B., and Grieve, R. Generic Oceanographic array technologies (GOATS 98)- Bi-static seabed scattering measurements using autonomous underwater vehicles. SACLANTCEN SR 302, La Spezia, Italy, SACLANT Undersea Research Centre, October 1998.

[23] Hovem, J.M. Detection of buried objects in the sea bed. SACLANTCEN SR 279, La Spezia, Italy, SACLANT Undersea Research Centre, 1998.

[24] Fioravanti S, Maguer, A, Lovik, A. A parametric synthetic aperture sonar for the detection of proud and buried mines. SACLANTCEN SR 268, La Spezia, Italy, SACLANT Undersea Research Centre, 1997.

[25] Sheriff, R.W., Synthetic aperture beamforming with automatic phase compensation for high-frequency sonars. Proc. IEEE Symposium on AUV technology, pp 236–245, Washington DC, June 1992

[26] Pinto, M.A, Fohanno, F., Tremois, O., Guyonic, S. Autofocusing a synthetic apreture sonar using the temporal and spatial coherence of seafloor reverberation, in *High Frequency Acoustics in Shallow Water* (Pace, N. G., Pouliquen, E., Bergem, O. and Lyons, A. P. eds.), SACLANTCEN CP-45, 417-424, NATO SACLANT Undersea Research Centre, 1997.

[27] Schmidt, H. Physics of 3-D scattering from rippled seabeds and buried targets in shallow water", SACLANTCEN SR 289, La Spezia, Italy, SACLANT Undersea Research Centre, 1998.

[28] Muir, T.G. Non linear parametric transduction in underwater acoustics, IEEE Ultrasonic Symposium Proceedings, 1974

[29] Osborne, M. F. M. and Hart, S. D. Transmission, reflection, and guiding of an exponential pulse by a steel plate in water. i. Theory, *Journal of the Acoustical Society of America*, 17, 1945: 1-18.

[30] Quentin, G. and Talmant, M. The plane plate model applied to the scattering of the ultrasonic waves from cylindrical shells, in *Elastic wave propagation* (M. F. McCarthy and M. A. Hayes, eds.), 477-482, Elsevier Science, North-Holland, 1989.

[31] Sessarego, J.P, Sageloli, J., Gazanhes, C. and Überall, H. Two Scholte-Stoneley waves on doubly fluid-loaded plates and shells, *Journal of the Acoustical Society of America*, 101, 1997: 135-142.

[32] Veksler, N. D. *Resonance Acoustic Spectroscopy.* Berlin: Springer Verlag, 1993.

[33] Flax, L, Dragonette, L.R and Überall, H. Theory of elastic resonance excitation by sound scattering, *Journal of the Acoustical Society of America*, 63, 1978: 723-731.

[34] Rumerman, M. L. Contribution of membrane wave reradiation to scattering from finite cylindrical steel shells in water, *Journal of the Acoustical Society of America*, 93, 1993: 55-65.

[35] Tesei, A., Fox, W.L.J., Maguer, A, Lovik A. Resonance scattering analysis by autoregressive models applied to air-filled cylindrical thin walled shells in water. SACLANTCEN SR 265, La Spezia, Italy, SACLANT Undersea Research Centre, 1997.

[36] Tesei, A., Fawcett, J.A., Fox, W.L.J., Maguer, A. Resonance analysis of the acoustic response of a water-filled cylindrical shell. SACLANTCEN SR 295, La Spezia, Italy, SACLANT Undersea Research Centre, 1998.

[37] Tesei, A., Fox, W.L.J., Maguer, A., Lovik, A. A method of target characterization based on the analysis of Scholte-Stoneley and Lamb-type waves scattered by submerged fluid-filled thin-walled shells. Journal of the Acoustical Society of America, 103, 1998:2813. Seattle

[38] Barnsley, M. F., Devaney, R. L., Mandelbrot, B. B., Peitgen, H. O., Saupe, D and Voss, R. F. *The Science of Fractal Images.* New York: Springer-Verlag, 1988.

[39] Peitgen, H.O and Saupe, D. The science of fractal images. *Springer Verlag, New-York*, 1988.

[40] Robertsson, J.O.A., Blanch, J.O. and Symes, W.W. Viscoelastic finite-difference modeling. *Geophysics 59*, 1994: pp 1444-1456.

[41] Fawcett, J.A, Grimbergen, J.L.T. Finite difference modelling of scattering by objects in the sea bed, SACLANTCEN SR 256, La Spezia, Italy, SACLANT Undersea Research Centre, 1996.

[42] Zerr, B., Tesei, A., Maguer, A., Fox, W.L.J., Fawcett, J.A. Target classification methodology combining reconstruction from multiple aspects and resonance scattering analysis. Proceedings of the fourth European conference on underwater acoustics, pp.813-818, 21-25 September, 1998. Rome

[43] SACLANTCEN Annual report 1998.

[44] Hermann, G.T. *Image Reconstruction from Projection.* Academic Press, New York, 1980.

[45] Mersereau, R.M. and Oppenheim, A.V. Digital reconstruction of multidimensional signals from their projections. *Proceedings of the IEEE*, 62, 1974: 1319-1338.

[46] Jain, A.K. *Fundamental of Digital Image Processing.* Englewood Cliffs, NJ, Prentice Hall, 1989: 431-475.

[47] Zerr, B and Stage, B. Three-dimensional reconstruction of underwater objects from a sequence of sonar images. *IEEE International Conference on Image Processing*, Lausanne 16-19 September, 1996.

[48] Fox, W.L.J., Fawcett, J. A., Jourdain-Albonico, D and Tesei, A. Measurements of free-field acoustic scattering from cylindrical shells. SACLANTCEN SM 331, La Spezia, Italy, SACLANT Undersea Research Centre, 1997.

[49] Tesei, A., Maguer, A., Fox, W.L.J., Schmidt, H. Measurements of acoustic scattering from partially and completely buried spherical shells. SACLANTCEN SM 362, La Spezia, Italy, SACLANT Undersea Research Centre, 1999

[50] Lim, R., Lopes, J. L., Hackman, R. H. and Todoroff, D. G. Scattering by objects buried in underwater sediments: Theory and experiment," *Journal of the Acoustical Society of America*, 93, 1993: 1762-1783.

[51] Lim, R. Scattering by partially-buried shells, *Joint ICA/ASA conference*, 1998: 501-502, Seattle.

[52] Urick, R. J. *Principles of Underwater Sound.* New York: McGraw Hill, third ed., 1983.

[53] Bentech Subsea AS, Stjørdal, Norway, *TOPAS PS040 Operator Manual.*

[54] Bergem, O., Pace, N. G. Calibration of the TOPAS PS040. Part I: Measurements recorded with TOPAS acquisition system," SACLANTCEN SM 119, La Spezia, Italy, SACLANT Undersea Research Centre, 1996.

[55] Fioravanti, S., Maguer, A., Fox, W. L. J., Gualdesi, L., and Tesei, A. Underwater rail facility for highly controlled experiments at sea. Third European MAST Conference, Lisbon, Portugal, 1998.

Annex A
EXPERIMENTAL SETUP

The parametric sonar used in the various reported experiments was the SIMRAD TOPAS (TOpographic PArametric Sonar). Its center primary frequency is 40 kHz, and it generates secondary frequencies in the range 2–16 kHz [13].

A short single pulse is obtained by transmitting a weighted HF-burst at the primary frequency. The TOPAS transducer [53, 54] consists of 24 staves, electronically controlled to form a beam in a selected direction. The transmitting source level is approximately 238 dB for the primary frequency. The source levels obtained at different frequencies vary from about 190 to 207 dB ref. μPascal at 1 m in the 2 to 16 kHz frequency band. Figure 32 gives an example of the generated signal (in time and frequency) at the secondary frequency of the TOPAS sonar as received on an hydrophone suspended in the water column.

In order to acquire data from various source-receiver geometries, the transmitter was mounted on a 10 m high tower (as shown on Fig. 33). The tower in turn was mounted on a 24 m linear rail on the bottom, along which its position could be precisely controlled. The TOPAS transmitter was mounted in a Pan-and-Tilt assembly with a MRU (Motion Reference Unit) so that the transmission direction could be accurately measured [55].

A common experimental configuration for the penetration measurements and the buried mine detection measurements is shown in Fig. 34.

For one of the subcritical penetration experiment, an array of 14 buried hydrophones was deployed in the seabed. The hydrophones were mounted on 5 vertical poles as shown in Fig. 35. The burial depths of the hydrophones varied from 5 cm to 52 cm. The central pole had one hydrophone mounted above the seabed to measure the incident field.

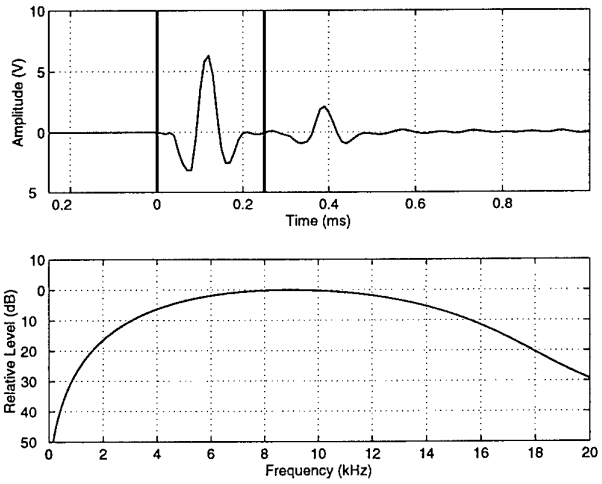

Figure 32 *Example of a signal recorded on the hydrophone in the water (top). The direct path signal (between 0 and 0.25 ms) is considered as a reference transmit signal for further processing, and is shown in the frequency domain in the bottom plot. The other signal centered at 0.4 ms is due to the bottom bounce path.*

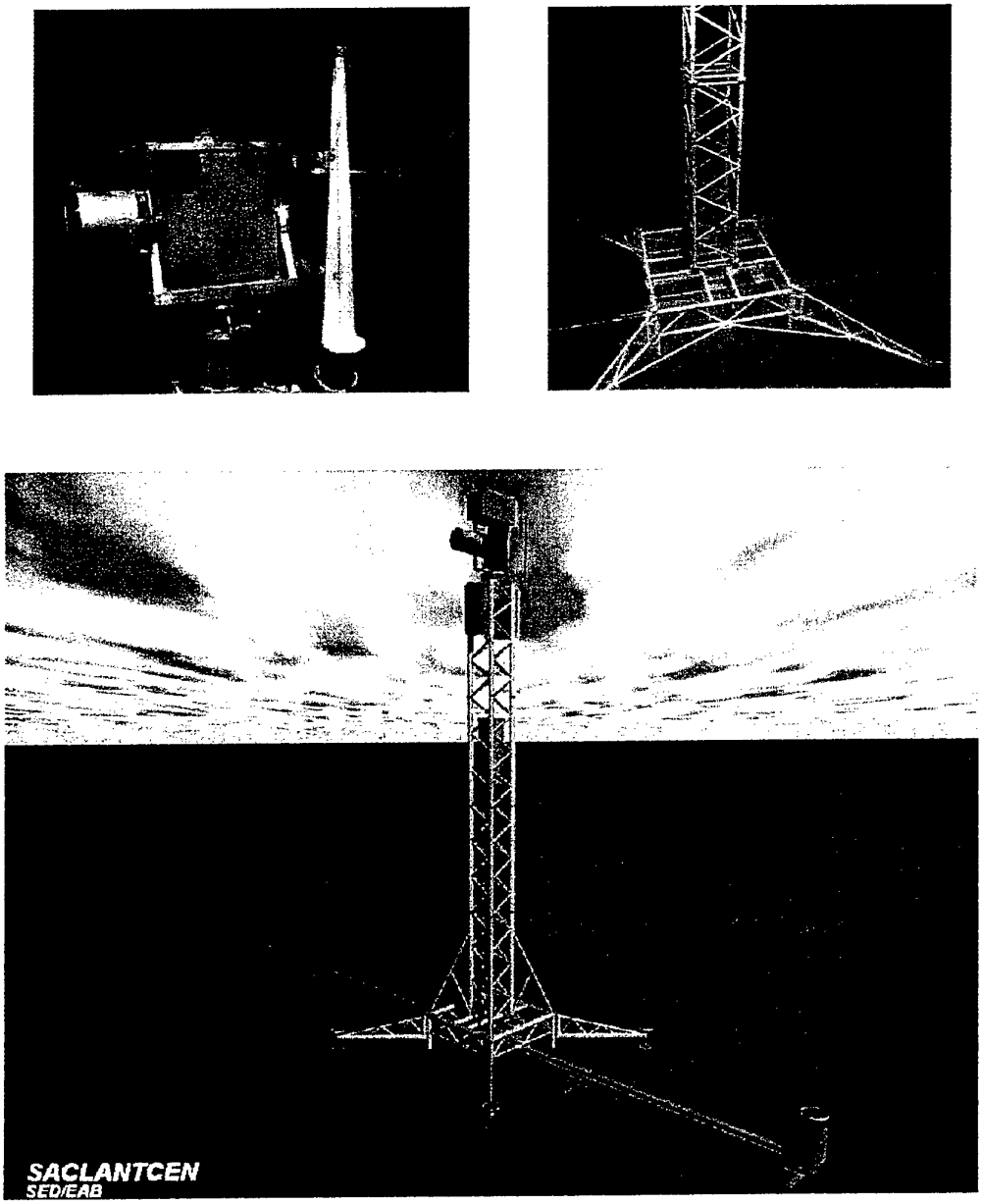

Figure 33 *Portable underwater rail designed to acquire data under very accurate source-receiver geometries. The transmitter is mounted on a 10 m tower, which in turn is mounted on a 24 m linear rail, along which the transmitter position can be precisely controlled. The TOPAS transmitter is mounted in a pan-and-tilt assembly with a MRU (motion reference unit) which permits accurate measurement of the transmission direction.*

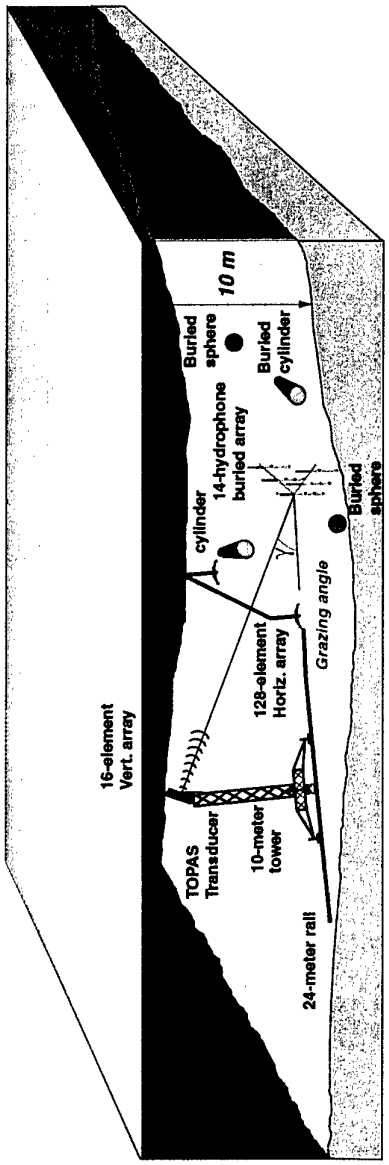

Figure 34 *Experimental configuration for penetration and buried mine detection/classification measurements. A parametric source is mounted on a 10 m tall tower which can be repositioned on a rail on the seabed to vary the angle of incidence. A 14-hydrophone buried array is used for the penetration measurements. A 16-element vertical array receives the backscattering data from the buried targets in monostatic conditions. A 128-element horizontal array receives the backscattering data from the buried targets in bistatic conditions.*

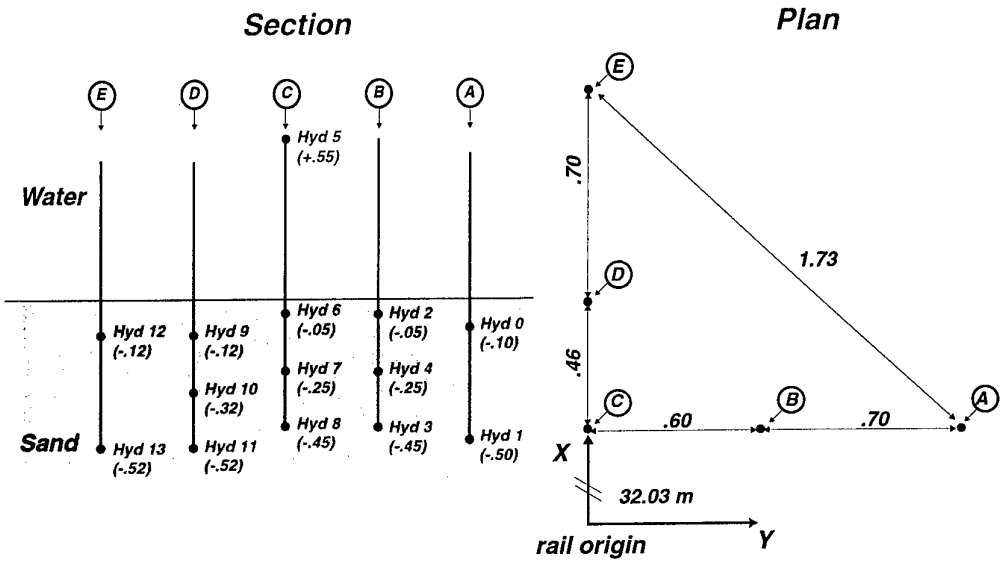

Figure 35 *14-hydrophone Reson TC4034 array geometry. The array is divided in 5 vertical poles A,B,C,D and E. The x-coordinate gives horizontal distance between rail end and each hydrophone. The y-coordinate gives distance between the rail axis and the hydrophone. The z-coordinate (depth) is given for each hydrophone in the section.*

Document Data Sheet

Security Classification		Project No.
UNCLASSIFIED		03-A
Document Serial No.	**Date of Issue**	**Total Pages**
SR-315	July 1999	74 pp.

Author(s)

Maguer, A., Fox, W.L.J., Zerr, B., Tesei, A., Bovio, E., Fioravanti, S.

Title

Buried mine detection and classification (Research Summary 1996-1999)

Abstract

The applicability of low-frequency sonar (2-16 kHz) to buried mine detection has been investigated. Experiments were performed on sound penetration into sediment, buried target detection and broadband multiple aspect classification. The results of the experiments are given in this report and compared with modelled results.

One of the main results is our success in understanding the physical mechanisms contributing to subcritical penetration into sediment. It has been demonstrated that the evanescent wave was dominant in the lower frequencies [2-5 kHz] of our bandwidth of interest [2-16 kHz]. Roughness scattering dominates at higher frequencies (above 5 kHz) for our bottom type (RMS roughness 1.5 cm, cross-ripple correlation length 25 cm). Although roughness scattering has been shown to be one mechanism for explaining "anomalous" penetration into sediment, its potential for detection and classification of buried objects is unclear due to the low level and the lack of coherence of the received signals. It is demonstrated that sound speed variation with frequency, could exist for permeable sandy bottoms, which could influence the design of a buried mine sonar.

The detection of buried targets is shown to be very effective at above the critical angle. At subcritical angles, detection becomes difficult. Significant gains in signal-to-reverberation radio below critical angle were obtained either by emphasizing a relatively narrow band of frequencies at the lower end of the transmitted bandwidth (below 3 kHz) or by using a larger physical array or synthetic array processing which improve the sonar resolution. Simulations have shown that lower frequencies (of the order of 0.5-1 kHz) are essential to the detection of buried targets at low grazing angles and that the de3tection at those frequencies will only be effective for shallow buried targets.

A method based on multiple-aspect target echo analysis in time and frequency domains, which considers the rigid and resonance responses is presented. Its potential was demonstrated in simulation and on real data (exercise mine, cylinders and rocks) for proud targets and for buried spheres.

Keywords

Seafloor scattering – sound penetration – Kirchhoff theory – small perturbation theory – evanescent wave – detection – synthetic aperture processing – target classification – tomography – resonance scattering analysis – target scattering modelling - minehunting

Issuing Organization

North Atlantic Treaty Organization
SACLANT Undersea Research Centre
Viale San Bartolomeo 400, 19138 La Spezia, Italy

[From N. America: SACLANTCEN (New York) APO AE 09613]

Tel: +39 0187 527 361
Fax:+39 0187 527 700

E-mail: library@saclantc.nato.int